

# Language Model Planning from an Information Theoretic Perspective

Muhammed Ustaomeroglu\*<sup>1</sup> Baris Askin\*<sup>1</sup>

Gauri Joshi<sup>1</sup> Carlee Joe-Wong<sup>1</sup> Guannan Qu<sup>1</sup>

\*Equal contribution, <sup>1</sup>Carnegie Mellon University

## Abstract

The extent to which decoder-only language models (LMs) engage in planning, that is, organizing intermediate computations to support coherent long-range generation, remains an open and important question, with implications for interpretability, reliability, and principled model design. Planning involves structuring computations over long horizons, considering multiple possible continuations, and selectively reusing past information, but how effectively transformer-based LMs realize these capabilities is still unclear. We address these questions by analyzing the hidden states at the core of transformer computations, which capture intermediate results and act as carriers of information. Since these hidden representations are often redundant and encumbered with fine-grained details, we develop a pipeline based on vector-quantized variational autoencoders that compresses them into compact summary codes. These codes enable measuring mutual information, allowing systematic analysis of the computational structure underlying model behavior. Using this framework, we study planning in LMs across synthetic grammar, path-finding tasks, and natural language datasets, focusing on three key aspects: (i) the planning horizon of pre-output computations, (ii) the extent to which the model considers alternative valid continuations, and (iii) the reliance of new predictions on earlier computations. By answering these questions, we advance the understanding of how planning is realized in LMs and contribute a general-purpose pipeline for probing the internal dynamics of LMs and deep learning systems. Our results reveal that the effective planning horizon is task-dependent, that models implicitly preserve information about unused correct continuations, and that predictions draw most on recent computations, though earlier blocks remain informative.

## 1 Introduction

Language models (LMs) have advanced so rapidly that they now engage in open-ended conversation, write functional code, and even solve challenging mathematical problems [1, 9, 20, 55]. Beyond these raw capabilities, scaffolding and augmentation techniques further enhance reasoning and planning [7, 46, 63–65]. In parallel, hybrid systems integrating LMs with symbolic planners or external tools have achieved state-of-the-art performance in embodied and tool-use domains [48, 60, 67].

All the above success suggests that LMs have a certain capability of “planning ahead,” similar to what humans do in generating coherent long speeches and long-horizon problem solving. Yet, the typical training method for LMs, next token prediction, focuses only on predicting the next token, which seemingly suggests LMs are myopic. Motivated by this contrast, this paper seeks to understand the planning behavior of LMs and how it is affected by next-token prediction (NTP) vs. multi-token prediction (MTP) in training. As “planning behavior” is a broad term that has many facets, we further narrow our focus to the following three canonical aspects of planning. First, good planners are *forward-looking*.

They structure intermediate computations over a receding horizon so that near-term actions serve longer-term objectives, an idea made explicit in model-predictive control (MPC) and world-model-based approaches [22, 28, 35, 38]. Second, good planners are *branch-aware*. Before committing, they keep multiple plausible futures “alive,” comparing candidates rather than greedily following a single line, an ability central in classical MPC and world-model-based control methods [23, 35, 38], and closely tied to robustness under paraphrase and logically related prompts [2, 32, 45] and to the success of search-based scaffolds such as Tree- and Graph-of-Thoughts [7, 65]. Third, good planners are *stateful*. They reuse and build upon earlier computations so that later decisions depend coherently on what has already been processed. In classical planning and control, this corresponds to carrying forward simulated states, costs, or latent variables across the planning horizon so that each new action is consistent with past predictions [35, 38]. Given the above three aspects about planning, this paper seeks to understand,

*To what extent are LMs forward-looking, branch-aware, and stateful?  
How does the training method (NTP vs. MTP) affect these qualities?*

We approach the above questions by studying the *internal states and computations* of an LM, as recent work shows that transformers internally encode rich, high-level abstractions such as belief states, game configurations, and world models that extend far beyond their immediate outputs, and that these abstractions can be partially extracted [29, 41, 44, 47]. This makes the internal representations of LMs a natural locus for investigating how they plan and reason. While not aimed at these specific questions, existing methods have explored internal computations of models, e.g. using probing classifiers to test for linguistic features in hidden states or mechanistic analyses to identify circuits and disentangled features within transformers [8, 15, 25]. However, these only indirectly relate to our questions, and despite important progress, these strategies have clear limitations. Circuit discovery requires heavy manual engineering [10, 15, 36, 61], while probing risks conflating genuine representations with probe artifacts [25–27, 42, 58]. These limitations necessitate new approaches towards understanding the internal computations that are automated, scalable, and less susceptible to probing’s confounding of representations learned by the probe with those in the model itself.

**Contribution 1: An information-theoretic tool towards understanding internal states of LMs:** In contrast to prior works in mechanistic interpretability or probing methods, we propose a framework to study how planning-related computations are organized inside LMs that is both *automated* (no manual circuit engineering) and *free from confounding* caused by learned probes. Specifically, (a) to avoid confounding caused by the probe, we propose to calculate the *Mutual Information* (MI) between two components of the LMs, which provides a lens on how planning-related information is organized. For example, to understand the “forward-looking” question, the MI between the internal states of the prefix and that of future generations can shed light on how much computations inside LMs plan ahead for future tokens. In contrast, probing detects whether a piece of information is present in a LM hidden state by training an external model to predict the information from the hidden state, which may introduce additional representational power brought by the external model. On the other hand, the MI is a confound-resistant metric measuring how much two variables contain information about each other, which avoids confounding by not introducing a new model. Moreover, unlike correlation, which is sensitive primarily to linear relationships under a chosen parameterization, MI captures arbitrary statistical dependence and is symmetric and invariant under invertible reparameterizations. (b) To make the MI calculation *scalable* to potentially very high dimensional hidden state vectors, we employ a Vector-Quantized Variational Autoencoder (VQ-VAE) to map collections of block outputs into discrete codes that serve as coarse summaries of internal states [57]. We use VQ-VAE as a practical and suitable compressor with a discrete codebook and transformer encoder, enabling MI estimation over variable-sized blocks; our validation study (App. A.3) supports this choice. We calculate MI between the coarse summaries instead of the raw hidden states. This step is crucial: fine-grained activations are high-dimensional and redundant, making a detailed direct analysis infeasible, while the compressed codes capture the salient distinctions necessary for comparing computations across layers, positions, and contexts.

While our framework is general and could be applied to other applications in deep learning, such as disentangling reasoning circuits in multimodal architectures or characterizing information flow in reinforcement learning (RL), in this work, we use it to analyze the planning of transformer models, which we introduce below.

**Contribution 2: Understanding the planning of LMs.** Using the information-theoretic framework, we analyze LMs’

ability to be (i) forward-looking, (ii) branch-aware, and (iii) stateful in decoder-only transformers, across a symbolic task, a structured reasoning problem, and natural text (§ 3):

- **Horizon of the Plan** (§ 3.1): how far ahead a model plans before producing its next token.
- **Branching in the Plan** (§ 3.2): to what extent a LM internally considers alternative responses.
- **History in the Plan** (§ 3.3): to what extent the token generation relies on earlier computations.

Our results show that planning is task-contingent and weakly modulated by the training objective loss, i.e., MTP versus NTP. When the task demands a longer horizon, the LM’s pre-output states retain information about tokens beyond the immediate next step. In contrast, in locally syntactic settings, this dependence concentrates near the next token. Training with MTP loss modestly reduces purely myopic behavior. Internally, the model encodes alternatives to the produced answer, and the strength of this branching awareness of the plan varies with task difficulty and model quality. Finally, next-token decisions draw most strongly on the last layers and the most recent token indices, yet earlier blocks retain nontrivial information, indicating stateful computation.

**Related work.** Despite the recent advances in LM planning abilities [7, 46, 48, 60, 63–65, 67], recent studies highlight that significant challenges remain, and current approaches to LM planning still fall short of fully addressing complex reasoning and decision-making tasks. For example, [32] show that models can produce conflicting answers under logically related prompts despite local plausibility, which shows lack of long-horizon planning although short-horizon it works fine; [2, 37, 45, 62] highlight inconsistencies in the model’s outputs and struggles with planning tasks. Taken together, these findings underscore that understanding whether and how planning arises in LMs is not only an open empirical challenge, but also central to both their interpretability and the principled design of future model architectures.

To interpret LMs, some approaches treat the model as a black box and design tasks or benchmarks to gauge reasoning, robustness, or generalization abilities at a behavioral level [30, 51]. While such evaluations provide useful insights, they miss several perspectives that can be gained by examining the internal mechanisms of the model. In contrast, mechanistic interpretability seeks to reverse-engineer transformer computations into human-understandable parts, treating the residual stream as the main information pathway and attention heads as separate components that pass information along [8, 12, 14, 15, 25, 33, 40]. However, circuit discovery requires significant manual engineering [10, 36, 61]. Beyond empirical tools, mathematically grounded perspectives also shed light on transformer and LLM interpretability [3, 16, 34, 56], yet these approaches are often criticized for lacking a one-to-one correspondence with experimental results, since their proofs typically rely on strong assumptions that may not hold for the highly non-smooth LM architectures. In contrast to them, our method (§ 2) enables the study of LMs both behaviorally and structurally, by examining their internal mechanisms, without the need for labor-intensive circuit discovery or strong assumptions on the LM. Still, due to its reliance on information-theoretic tools, our approach can only capture aggregate phenomena, providing insights in an average sense rather than interpreting individual input prompts.

A different line of interpretability work views LM hidden states as structured representations that can be "probed"—probing refers to training lightweight models, often linear classifiers, to read out specific information from hidden states in order to test what the model represents internally. Using probing, researchers have shown that transformer hidden states encode structured belief-state and world-model-like information [21, 24, 47]. Other works demonstrate that a single hidden state can carry information about multiple future tokens [41] and that probing can reveal the underlying algorithms LLMs use to solve tasks [4]. However, standard accuracy-based probing has been criticized for combining what the probe can learn with what the representation actually encodes, making the results sensitive to probe capacity, data size, and hyperparameters [25, 42]. Further, high probe scores often come from exploiting superficial linear context cues rather than genuine structural knowledge [27]: probing can even reveal features that a model does not use for its task [26, 43]. Consequently, some critiques motivate adopting information-theoretic lenses [13, 58]. Similar to some of these information-theoretic approaches [49, 50, 54, 59], our method makes use of information theory. For a more detailed discussion of related work, please refer to App. C.

## 2 Method

Given a prefix sequence of length  $T$ ,  $\mathbf{x}_{1:T} = [x_1, x_2, \dots, x_T]$ , the decoder-only LM,  $\mathcal{M}$ , generates subsequent tokens  $\{\hat{x}_{T+\tau} \mid \tau = 1, 2, \dots\}$  autoregressively. We denote the hidden activation at  $t$  after the  $\ell^{\text{th}}$  transformer layer by  $h_t^\ell \in \mathbb{R}^d$  where  $d$  is the hidden dimension of the model.

In our analysis, we treat the outputs  $h_t^\ell$  of individual transformer blocks as the fundamental units of computation<sup>1</sup>. We posit that a block’s output is informative about the computation performed within that block [15, 29, 33, 41, 47]. We use them as a proxy for the model’s internal processing since each block’s computation contributes to the overall function of the model. To analyze how planning emerges in the model’s internal dynamics, we examine collections of layer–token indices  $\mathcal{S}$  and aggregate the corresponding block outputs as  $G_{\mathcal{S}} = \{h_t^\ell \mid (\ell, t) \in \mathcal{S}\}$ , a representation for the computations within its block. While  $G_{\mathcal{S}}$  provides a fine-grained representation of block computations, it often contains unnecessary details for our planning analysis. Hidden states may encode small variations due to token positions, normalization shifts, or attention noise, factors that are critical for exact output reconstruction but irrelevant for studying planning structure. Moreover, MI estimates between such high-dimensional vectors have high variance and are hard to find. To address both issues, we construct coarse, discrete representations of  $G_{\mathcal{S}}$ . These abstractions preserve the structural dependencies required for our analysis while filtering out irrelevant micro-level variability, yielding more stable and interpretable MI estimates.

**Measuring mutual information between coarse representations.** To investigate how planning is realized within the model, we use MI as a principled way to quantify relationships between the coarse representations of different computations. Suppose we focus on two hidden state blocks,  $G_A$  and  $G_B$ , which are random variables depending on the data distribution and the trained model parameters. We denote their coarse, discrete representations by  $Z_A \in \mathcal{Z}_A$  and  $Z_B \in \mathcal{Z}_B$  where  $\mathcal{Z}_A$  and  $\mathcal{Z}_B$  are the finite alphabets of possible codes. For realizations  $z_a \in \mathcal{Z}_A$  and  $z_b \in \mathcal{Z}_B$ ,  $p(z_a, z_b)$ ,  $p(z_a)$ , and  $p(z_b)$  refer to the joint probability of  $Z_A$  and  $Z_B$ , and the marginal probabilities of  $Z_A$  and  $Z_B$ , respectively. Mutual information, which measures how much knowing  $Z_A$  reduces uncertainty about  $Z_B$  (and vice versa), is defined as,

$$I(Z_A; Z_B) = \sum_{z_a \in \mathcal{Z}_A} \sum_{z_b \in \mathcal{Z}_B} p(z_a, z_b) \log \frac{p(z_a, z_b)}{p(z_a)p(z_b)}. \quad (1)$$

Since the true data distribution is inaccessible, we approximate by replacing  $p(z_a)$ ,  $p(z_b)$ , and  $p(z_a, z_b)$  in Eq. 1 with their empirical estimates from the datasets. We further define normalized mutual information (nMI) metric as

$$\text{nMI}(Z_A; Z_B) = \frac{I(Z_A; Z_B)}{I_{\max}}. \quad (2)$$

where  $I_{\max}$  denotes the maximum value across the set of MI calculations performed in the same experimental analysis for comparison. For our purpose of LM planning investigation, the nMI metric is sufficient since our analyses depend on relative, rather than absolute, comparisons between sets of computations. Absolute values can be misleading for three reasons: (i) the estimated MI of coarse representations is bounded above by the logarithm of the alphabet size, making it inherently dependent on the experimental choice; (ii) any coarse-graining necessarily discards some information, which is advantageous for our setting as discussed but removes any meaning of absolute MI values related to the original hidden states; and (iii) answering our three research questions (§ 3) requires only relative comparisons of MI instead of relying on absolute values.

**Acquiring coarse representations.** To estimate MI between the high-level representations of hidden state blocks,  $G_{\mathcal{S}}$ , we need to find a mapping from  $G_{\mathcal{S}}$  to the discrete codes. The size of target layer-token indices  $\mathcal{S}$  and its corresponding activation outputs  $G$  may vary depending on the analysis. For instance, when examining all block outputs across the prefix tokens,  $\mathcal{S}$  spans every layer and grows with the prefix length  $T$ . Since neural networks are good at learning representations, we employ an encoder-decoder neural network architecture: the encoder maps the potentially long

<sup>1</sup>We use the terms “hidden state” and “(hidden) activation” interchangeably to refer to these outputs.

and variable-sized  $G$  into a compact representation, and the decoder aims at recovering  $G$  from it. Leveraging the effectiveness in handling variable-length inputs and learning rich representations [31], we adopt transformer-based encoder and decoder models. Specifically, we employ Vector-Quantized Variational Autoencoders (VQ-VAEs; Van Den Oord et al. 57) framework. VQ-VAE is a framework consisting of an encoder-decoder network with a trainable embedding codebook between them to discretize the encoder’s output. Its training objective consists of a reconstruction loss between the decoder’s output and the input signal, supplemented with auxiliary terms that encourage effective utilization and learning of the codebook embeddings. Overall, a VQ-VAE acts as a quantizer that extracts compact representations of the input by mapping to a codebook index. In addition to the vanilla VQ-VAE’s training objective, we introduce a cosine similarity loss across codebook embeddings to encourage representations assigned to different codes to diverge so that they are not only compact but also discriminative.<sup>2</sup> This enables embeddings to spread out in the latent space and ensures that codes capture distinct features of the data making them informative and discriminative. We refer reader to App. A.1 for the details of the implementation.

The trained encoder and the codebook of VQ-VAE are used to obtain coarse representations of transformer computations. Given a set  $G$  of block outputs corresponding to indices in  $\mathcal{S}$ , we map  $G$  to a discrete code in  $[K]$ , where  $K$  is the size of the codebook. Instead of fine-grained activations, we work with these high-level representation codes that serve as compact summary of complex internal computations in  $G$ . Importantly, we treat these codes not as semantically meaningful entities, but as representational summaries that allow us to find information relations. Therefore, the estimated nMI depends not only on the underlying relationship between the hidden state themselves, but also on how they are encoded to high-level codes. Our use of VQ-VAE ensures that the learned representations are nontrivial since the decoder achieves meaningful reconstructions, and the cosine similarity penalty enforces diversity among codebook embeddings, which is validated by the reconstruction quality and codebook similarity results presented in App. A.1. Furthermore, we validate that our framework can find a closer relation to a known underlying distribution, in a representative experimental setting. Due to space limits, we refer the reader to App. A.3 for the details and results of the validation experiment.

While our framework is general and could be applied to other applications in deep learning, in this work we use it to analyze how transformer models implement planning in practice, focusing on dimensions that are both theoretically meaningful and empirically informative.

### 3 Analysis of planning capability

We leverage our method to investigate three core aspects of the planning capabilities of LMs and their underlying computations: (3.1) how much a model plans about future tokens before producing its immediate prediction, (3.2) to what extent the model internally considers alternative correct continuations, and (3.3) to what extent the model relies on earlier computations within the context window when deciding the next tokens. In our analyses, we use architecture-matched GPT-3 Small [9] models employing rotary position embeddings [52]. We report results from multiple seeds.

**Training objectives: next-token vs. multi-token.** In our analysis, we examine two variants of LM training objectives:  $\mathcal{M}_{\text{NTP}}$  is trained with the standard next-token prediction (NTP) loss ( $\mathcal{L}_{\text{NTP}}$ ), which optimizes conditional likelihood of the immediate next token, and  $\mathcal{M}_{\text{MTP}}$  is trained with the multi-token prediction (MTP) loss ( $\mathcal{L}_{\text{MTP}}$ ), which encourages models to align their hidden states with predictions across multiple forthcoming tokens. Following [18] for MTP implementation, we use shared transformer layers and separate heads for the next tokens during training. During inference, both models use standard autoregressive next-token generation. Intuitively, NTP prioritizes local token-by-token

<sup>2</sup>In short, our VQ-VAE setting with the additional cosine loss combines the regularizing and contrastive approaches for representation learning, e.g., [11, 17]

consistency, whereas MTP incentivizes models to form short-horizon plans and reduces strictly myopic behavior [5, 39]. Both losses are described in detail in App. B.1.

**Datasets.** Our experiments span three datasets chosen to cover distinct aspects of planning. (i) *A context-free grammar (CFG) dataset* [4] emphasizes token-level rules and local coherence. Tokens in CFG carry intrinsic meaning, much like words in natural language, and are governed by both local and global syntactic constraints. The model’s task is to learn the grammar and predict valid next tokens that obey its rules. As a controlled substitute for natural language, CFG allows us to adjust vocabulary size and task difficulty, providing a clean environment for scientific study. (ii) *A path-finding (PF) task* (see Figure 1, right for illustration) requires models to generate valid paths between a fixed start and goal node in graphs with varying sizes and edge structures. The node vocabulary consists of 28 unique tokens, each representing a node identity. Unlike in CFG, these tokens do not carry intrinsic semantics and the meaning of a node token arises only through the set of edges it participates in. To construct language-model inputs, we linearize the graph by writing edges as pairs of adjacent node tokens separated by commas in a random order to prevent the model from exploiting positional shortcuts (e.g., “ $u v, r t, \dots$ ”). This edge-list representation ensures that the model must infer connectivity and graph structure rather than rely on token identity alone. Solving PF thus requires composing multiple reasoning steps over these relational inputs, analogous to chaining lemmas to form a proof, introducing a natural flavor of long-horizon planning. We construct two variants, PF-Short and PF-Long, which require finding paths of length 4 and 6 (including start and goal), respectively. (iii) *A natural language dataset*, OpenWebText [19], reflects real-world distributional modeling. Here the model predicts continuations consistent with natural text. These datasets cover a spectrum from low-level symbolic structure to high-level naturalistic text. We refer the reader to App. B.2 for details.

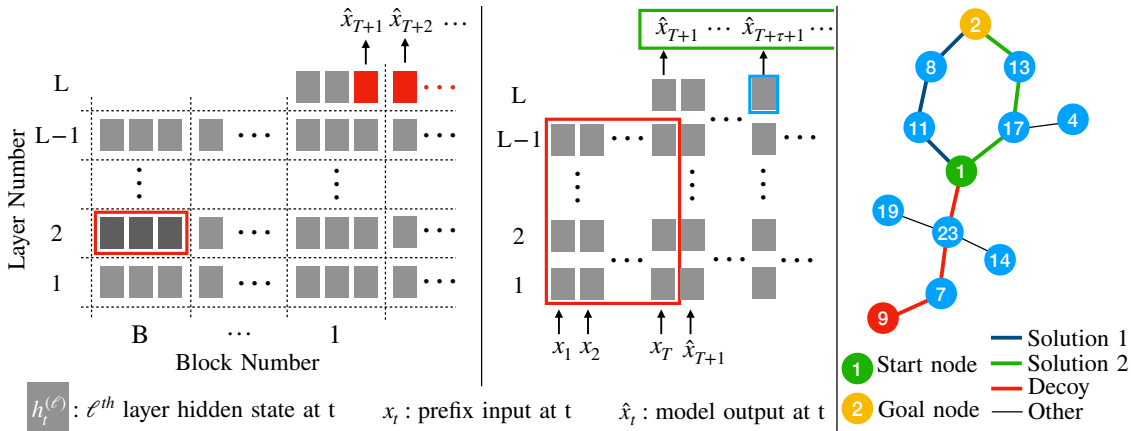


Figure 1: The visualizations of experimental settings. *Left:* History in the plan experiment (§ 3.3). *Middle:* Horizon of the plan and branches in the plan experiment (§ 3.1 & § 3.2). The red, blue, and green colors indicate target variables used in our analysis in *left* and *middle* panels. *Right:* An illustration of a simplified sample in PF task. Graphs and token numbers are randomly generated except for the start (1) and goal node (2). A sample prompt is “19 23 , 13 2 , 11 8 , 4 17 , 1 23 , 9 7 , 2 8 , 17 1 , 13 2 , 14 23 , 23 7 , 1 23 :” and correct responses are “1 11 8 2” or “1 17 13 2”.

### 3.1 Horizon of the plan

In autoregressive generation, predictions for tokens beyond the immediate next one depend on both the prefix and the model’s own generated outputs, which raises the question of how much computation the model allocates to tokens beyond the immediate prediction. We specifically ask:

*How much do LMs plan about future tokens before deciding on the immediate next token?*

To answer this question, we analyze two sets of activations. First, for a prefix of length  $T$ , we take the final-layer hidden states of the autoregressively generated tokens,  $h_{T+\tau}^L$  for  $\tau \geq 0$ . As  $h_{T+\tau}^L$  fully specifies the distribution over  $\hat{x}_{T+\tau+1}$ , we treat it as the model’s decision state and use its code  $Z_{T+\tau}^L$  as a concise summary of the strategy employed for that token, obtained from a trained VQ-VAE. Second, we collect all prefix activations across layers:

$$H = \{h_t^\ell \mid t = 1, \dots, T; \ell = 1, \dots, L-1\} \in \mathbb{R}^{T \times (L-1) \times d},$$

where  $H$  encodes the entirety of the model’s prefix computation that has an effect on future token generations. Training a separate VQ-VAE over  $H$ , we get the LM’s pre-output computation summary, and denote its high-level code as  $Z_{1:T}^{1:L-1}$ .  $H$  and  $h_{T+\tau}^L$  are respectively shown in red and blue colors in Figure 1 (left). We address our question by comparing how much the prefix computation’s summary  $Z_{1:T}^{1:L-1}$  tells us about the model’s decision state at the generated tokens. We measure the nMI between  $Z_{1:T}^{1:L-1}$  and  $Z_{T+\tau}^L$  for  $\tau \geq 0$  as defined in Eq. 2 with normalization  $\mathcal{I}_{\max} = \max\{\mathcal{I}(Z_{1:T}^{1:L-1}; Z_{T+n}^L)\}_n$ . If this ratio remains significantly above zero for large  $\tau$ , then the pre-output computation  $Z_{1:T}^{1:L-1}$  carries information on the strategy to produce  $\hat{x}_{T+\tau}$ , indicating the model’s initial prefix processing is not merely myopic but encodes forward-looking structure that persists into later generations. Conversely, if the ratio quickly decays to zero, then prefix computations primarily support only the immediate next prediction, with little evidence of planning ahead.

**Context-free grammar results.** We generate sentences of length  $[16, 67]$  from CFG rules, and for each sample select a prefix length  $T \in [8, 24]$  uniformly at random before, with the model generating the remaining continuation. For  $\mathcal{M}_{\text{NTP}}$  and  $\mathcal{M}_{\text{MTP}}$ , Figure 2a reports the nMI between  $Z_{1:T}^{1:L-1}$  and  $Z_{T+\tau}^L$  across  $\tau \geq 0$ . Because CFG tokens have intrinsic meaning and are significantly governed by local syntactic constraints, it is expected that prefix computations correlate most strongly with the first few generated tokens. Indeed,  $Z_{1:T}^{1:L-1}$  retains the highest information about the decision state for  $\tau = 0$ , and by  $\tau = 10$  the nMI drops to roughly one-fifth of its initial value. This indicates that the pre-output computation encodes a short-horizon plan tied mainly to the next few tokens.  $\mathcal{M}_{\text{MTP}}$  exhibits a similar pattern, with a slightly slower decay for  $\tau < 10$ , suggesting that the MTP loss does not substantially extend the horizon of pre-output computation in a model well-trained on CFG.

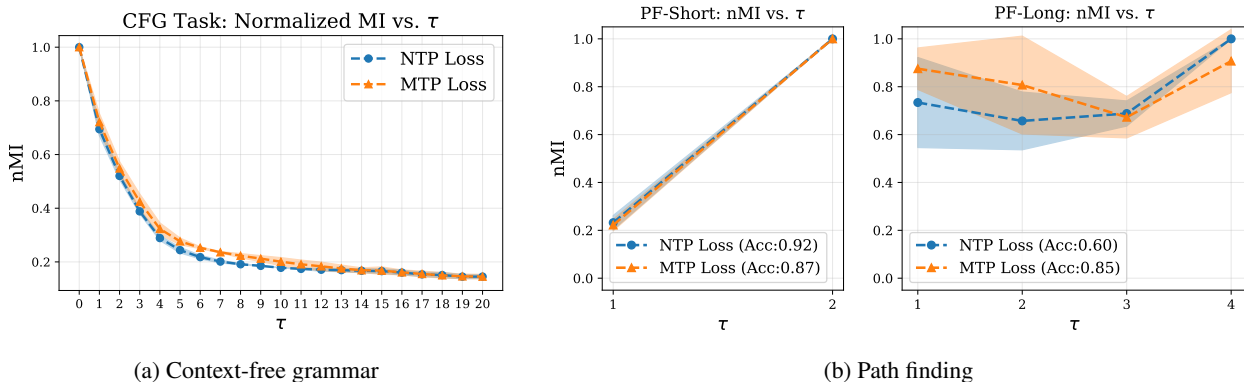


Figure 2: nMI results between the prefix summary codes and the last hidden state codes of generated tokens for CFG (a) and PF (b) tasks. nMI decays fast in CFG, showing short and local planning, while PF maintains or even increases nMI beyond  $\tau = 1$ , reflecting planning for later steps.

**Path finding results.** On PF-Short and PF-Long, we trained models on NTP and MTP losses. Because the start and end nodes are fixed tokens, the challenge lies in predicting the correct intermediate nodes ( $\tau = 1, 2$  for PF-Short and  $\tau = 1, 2, 3, 4$  for PF-Long) that connect them. We therefore focus our analysis on the intermediate positions and compute nMI as defined in Eq. 2. Figure 2b shows nMI across the generated path as well as the accuracy of correctly finding the whole path. For PF-Short, we see similar nMI trends across generated tokens for both  $\mathcal{M}_{\text{MTP}}$  and  $\mathcal{M}_{\text{NTP}}$ , which both attain high accuracy. Interestingly, prefix computations encode more information about the *second* intermediate node than about the first. A likely explanation is that there is less uncertainty about the final token given the edge information and that the model spares more pre-output computation to find the last token. This resembles a strategy

Table 1: Mean  $\pm$  std for  $\mathcal{I}(Z_H; Z_{\text{alt}}) / \mathcal{I}(Z_H; Z_{\text{decoy}})$  metric and accuracy values in branches in the plan experiment (§ 3.2). Models encode information about unchosen correct branches more strongly than unrelated decoys, indicating branch awareness in prefix computations.

Model	PF-Short		PF-Long	
	$\frac{\mathcal{I}(Z_H; Z_{\text{alt}})}{\mathcal{I}(Z_H; Z_{\text{decoy}})}$	Accuracy	$\frac{\mathcal{I}(Z_H; Z_{\text{alt}})}{\mathcal{I}(Z_H; Z_{\text{decoy}})}$	Accuracy
$\mathcal{M}_{\text{NTP}}$	$7.60 \pm 0.78$	$0.92 \pm 0.03$	$1.45 \pm 0.01$	$0.60 \pm 0.01$
$\mathcal{M}_{\text{MTP}}$	$6.29 \pm 0.17$	$0.88 \pm 0.05$	$1.82 \pm 0.27$	$0.85 \pm 0.02$

to work backwards from the goal, as a human solving this task might do. Similarly, for PF-Long, in Figure 2b, both  $\mathcal{M}_{\text{NTP}}$  and  $\mathcal{M}_{\text{MTP}}$  prefix computations encode a comparatively high amount of MI about the future tokens, unlike to the steady decay seen in CFG. This suggests that pre-output computations are not limited to the next token but also embed plans for upcoming positions, reflecting deliberate allocation of capacity toward future outputs. This finding is aligned with previous research on training LMs to exploit this reverse-solving approach, which has been shown to improve performance [5]. Taken together, these results indicate that LMs trained with both NTP and MTP loss can exhibit non-myopic behavior when trained on tasks that demand it. Lastly, in the PF-Long experiment, we observe that the nMI of  $\mathcal{M}_{\text{MTP}}$  is slightly more uniform across  $\tau$  than that of  $\mathcal{M}_{\text{NTP}}$ , which is a likely explanation for its higher accuracy by better predicting the earlier (harder) tokens along the generated path.

Overall, the dependency between pre-output summaries  $Z_{1:T}^{1:L-1}$  and decision states  $Z_{T+\tau}^L$  confirms that the planning horizon is task-dependent. On CFG, nMI drops quickly with  $\tau$  (short, local planning); on PF, it stays high and can peak beyond  $\tau = 1$ , allocating compute to later steps.

### 3.2 Branches in the plan

In many tasks, there can be multiple correct continuations for a given query. For example, a math problem may admit different solution strategies, or a natural language prompt may allow several equally valid completions. This raises the question of whether LMs, when producing one correct answer, also implicitly encode information about other possible correct answers. Specifically, for the subset of samples the model solves correctly, we ask:

*Does the model consider alternative correct answers when generating the next token?*

To investigate this question, we use the PF datasets, where each sample is constructed to have two correct paths and one decoy path (see App. B.2.2). By design, the correct paths and the decoy path do not share any common nodes, ensuring no correlation among them. Similar to § 3.1, we summarize prefix computations  $H$  into high-level codes  $Z_{1:T}^{1:L-1}$  using a VQ-VAE encoder. In addition, we train a separate VQ-VAE to encode an entire path to find codes for the alternative correct path ( $Z_{\text{alt}}$ ) and the decoy incorrect path ( $Z_{\text{decoy}}$ ).  $H$  and the generated path are visualized in Figure 1 (left) with red and green color, respectively. We then measure the MI between the prefix and alternative solution versus that between the prefix and decoy path through the ratio  $\mathcal{I}(Z_{1:T}^{1:L-1}; Z_{\text{alt}}) / \mathcal{I}(Z_{1:T}^{1:L-1}; Z_{\text{decoy}})$ . A ratio above one means that the prefix computations encode more information about the alternative path than the decoy, indicating branch awareness in pre-output planning.

Table 1 reports this ratio together with path-finding accuracy. On PF-Short, both  $\mathcal{M}_{\text{NTP}}$  and  $\mathcal{M}_{\text{MTP}}$  yield ratios well above 1 and high accuracy, showing that the prefix retains information about unused correct branches on easier instances. On PF-Long, the ratios are smaller yet remain above 1, which indicates attenuated but persistent branch information as path length grows.  $\mathcal{M}_{\text{MTP}}$  achieves both higher accuracy and a larger ratio than  $\mathcal{M}_{\text{NTP}}$ , suggesting that a model which solves the task more reliably also maintains richer branch-aware computation in its prefix states. Because the correct and decoy paths are disjoint, trivial overlap is ruled out as an explanation.

### 3.3 History in the plan

In an autoregressive LM, the final hidden state at the end of the prefix determines the next token, yet the computation producing it spans layers and earlier positions. This raises a natural question:

*To what extent do LMs rely on earlier computations when generating new tokens?*

To answer the question, we use an 8-layer decoder-only Transformer trained on OpenWebText with NTP objective. We estimate the nMI between the codes of the model’s decision state for the generated tokens and of blocks of prefix hidden state computations within the LM. Similar to § 3.1, we obtain a summary of the strategy employed for token  $\hat{x}_{T+\tau+1}$ , denoted  $Z_{T+\tau}^L$  with a VQ-VAE trained over the last layer of hidden states. We also partition each layer’s prefix hidden states into contiguous, non-overlapping blocks of length 16 and train a VQ-VAE to acquire the code  $\mathbf{B}_k^\ell$  where the block index  $k \in \{1, \dots, 12\}$  denotes the  $k^{\text{th}}$  block from the end of the prefix (i.e.,  $k = 1$  corresponds to the most recent 16 time steps before generation). In Figure 1 (middle), a sample block and a sample last hidden state are illustrated. We quantify the dependence between the codes of each computation block and the decision state by measuring nMI between  $\mathbf{B}_k^\ell$  and  $Z_{T+\tau}^L$  across all layers  $\ell$  and blocks  $k$ , as defined in Eq. 2, with  $\mathcal{I}_{\max} = \max\{\mathcal{I}(\mathbf{B}_k^\ell; Z_{T+n}^L)\}_{\ell,k,n}$ . Heatmaps in Figure 3 (left and middle) show the results for  $\tau = 0$  and 1 (see App. B.5.1 for  $\tau > 1$ ).

We observe that last layer computations retain the most information about the decision state of both immediate and future tokens which is aligned with the results of [41] and consistent with the design choice of assigning longer attention spans to higher layers [6, 53]. Furthermore, along the block axis, we observe a clear recency effect across all layers: the codes of the most recent blocks, i.e., final time steps of the prefix, computations ( $Z_1$ ), exhibit the highest nMI (Eq. 2) with the decision state of the generated tokens, and the nMI decays over earlier blocks in the prefix. Although analysis along both axes indicates that the LM primarily relies on the most recent computations, we still observe appreciable nMI in lower layers (small  $\ell$ ) and earlier blocks (large  $k$ ). This suggests that LMs retain information from earlier parts of the prefix when generating new tokens, instead of relying only on the most recent computations.

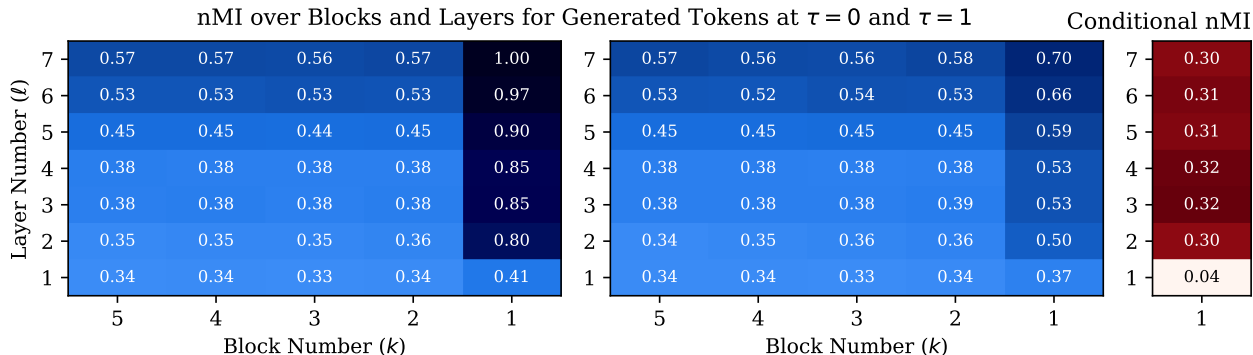


Figure 3: nMI across blocks and layers, and conditional nMI. *Left*: nMI between the hidden state block codes and the token decision state code at  $\tau = 0$ ,  $\text{nMI}(\mathbf{B}_k^\ell; Z_T^L)$ . *Middle*: nMI between block codes and the last-layer decision code at  $\tau = 1$ ,  $\text{nMI}(\mathbf{B}_k^\ell; Z_{T+1}^L)$ . In both heatmaps, nMI is higher for recent blocks (small  $k$ ) and final layers (high  $\ell$ ). *Right*: Conditional nMI for the 1<sup>st</sup> block,  $\text{nMI}(Z_{T-15:T-1}^\ell; Z_T^L | Z_T^\ell)$ , showing that most of the dependence between the 1<sup>st</sup> block and the generated token at  $\tau = 0$  is attributable to the final prefix position  $T$ .

We also define conditional normalized mutual information,  $\text{nMI}(Z_{T-15:T-1}^\ell; Z_T^L | Z_T^\ell)$  (see App. B.5.2 for details), where  $Z_{T-15:T-1}^\ell$  denotes the codes from layer  $\ell$  spanning prefix positions from  $T-15$  to  $T-1$ . This quantity, reported in Figure 3 (right), measures how much additional information about the decision state  $Z_T^L$  is captured by earlier time steps in the 1<sup>st</sup> block, beyond what is already contained in the final prefix position  $Z_T^\ell$ . The resulting values are approximately 0.3, which is much lower than the unconditional nMI values of the 1<sup>st</sup> block observed in the left heatmap. This gap suggests that the majority of the dependency between the 1<sup>st</sup> block and the decision state arises from the final prefix token at position  $T$ . This finding further reinforces our earlier conclusion: *the LM primarily relies on the most recent computations when generating new tokens.*

## 4 Conclusion

Drawing on a VQ-VAE, we develop an information-theoretic pipeline for compressing hidden-state trajectories into discrete codes and use them to compute MI between different parts of a LM’s computation. This coarse-grained view allows us to examine how much the prefix internal computations inform future prediction states, whether they preserve alternative continuations, and which blocks of history a decoder-only transformer relies on. Empirically, we compare training with standard NTP and MTP losses across a synthetic CFG task, PF tasks, and natural text. Our findings show that planning behavior varies with the task. In the CFG task, nMI between the prefix and decision state quickly decays, suggesting myopic computations. In path-finding, however, the prefix retains strong information about future steps and alternative correct paths, indicating branch awareness. We also observe a recency effect: decision states depend mainly on the final layers and most recent block, though earlier activations still carry some influence, with most of the dependence coming from the last prefix token. Taken together, these results suggest that LMs perform planning, but the extent and nature of that planning are contingent on the task and training objective. Our VQ-VAE-based MI framework provides an automated way to investigate such behaviors. Future work could extend this analysis to chain-of-thought-style training and RL-fine-tuned LMs, and investigate how architectural modifications can encourage planning.

**Acknowledgements.** This work was partially supported by the US National Science Foundation under grants CCF 2045694, CNS-2112471, CPS-2111751, and ONR N00014-23-1-2149 to GJ. In addition, the work was supported by NSF Grants 2154171, CAREER Award 2339112, CMU CyLab Seed Funding. This work used PSC Bridges-2 GPU at Pittsburgh Supercomputing Center through allocation CIS250226 from the Advanced Cyberinfrastructure Coordination Ecosystem: Services & Support (ACCESS) program, which is supported by US National Science Foundation grants #2138259, #2138286, #2138307, #2137603, and #2138296.

## References

- [1] Josh Achiam, Steven Adler, Sandhini Agarwal, Lama Ahmad, Ilge Akkaya, Florencia Leoni Aleman, Diogo Almeida, Janko Altenschmidt, Sam Altman, Shyamal Anadkat, et al. Gpt-4 technical report. *arXiv preprint arXiv:2303.08774*, 2023.
- [2] Jihyun Janice Ahn and Wenpeng Yin. Prompt-reverse inconsistency: LLM self-inconsistency beyond generative randomness and prompt paraphrasing. In *Second Conference on Language Modeling*, 2025. URL <https://openreview.net/forum?id=yfRkNRFLz1>.
- [3] Kwangjun Ahn, Xiang Cheng, Hadi Daneshmand, and Suvrit Sra. Transformers learn to implement preconditioned gradient descent for in-context learning. *Advances in Neural Information Processing Systems*, 36:45614–45650, 2023.
- [4] Zeyuan Allen-Zhu. ICML 2024 Tutorial: Physics of Language Models, July 2024. Project page: <https://physics.allen-zhu.com/>.
- [5] Gregor Bachmann and Vaishnavh Nagarajan. The pitfalls of next-token prediction. In *Forty-first International Conference on Machine Learning*, 2024. URL <https://openreview.net/forum?id=76zq8Wk16Z>.
- [6] Iz Beltagy, Matthew E Peters, and Arman Cohan. Longformer: The long-document transformer. *arXiv preprint arXiv:2004.05150*, 2020.
- [7] Maciej Besta, Nils Blach, Ales Kubicek, Robert Gerstenberger, Michal Podstawski, Lukas Gianinazzi, Joanna Gajda, Tomasz Lehmann, Hubert Niewiadomski, Piotr Nyczyk, et al. Graph of thoughts: Solving elaborate problems with large language models. In *Proceedings of the AAAI conference on artificial intelligence*, volume 38, pages 17682–17690, 2024.
- [8] Trenton Bricken, Adly Templeton, Joshua Batson, Brian Chen, Adam Jermyn, Tom Conerly, Nick Turner, Cem Anil, Carson Denison, Amanda Askell, Robert Lasenby, Yifan Wu, Shauna Kravec, Nicholas Schiefer, Tim Maxwell, Nicholas Joseph, Zac Hatfield-Dodds, Alex Tamkin, Karina Nguyen, Brayden McLean, Josiah E Burke, Tristan Hume, Shan Carter, Tom Henighan, and Christopher Olah. Towards monosemanticity: Decomposing language models with dictionary learning. *Transformer Circuits Thread*, 2023. <https://transformer-circuits.pub/2023/monosemantic-features/index.html>.
- [9] Tom et al. Brown. Language models are few-shot learners. In H. Larochelle, M. Ranzato, R. Hadsell, M.F. Balcan, and H. Lin, editors, *Advances in Neural Information Processing Systems*, volume 33, pages 1877–1901. Curran Associates, Inc., 2020.
- [10] Lawrence Chan, Adrià Garriga-Alonso, Nicholas Goldwosky-Dill, Ryan Greenblatt, Jenny Nitishinskaya, Ansh Radhakrishnan, Buck Shlegeris, and Nate Thomas. Causal scrubbing, a method for rigorously testing interpretability hypotheses. *AI Alignment Forum*, 2022. <https://www.alignmentforum.org/posts/JvZhhzycHu2Yd57RN/causal-scrubbing-a-method-for-rigorously-testing>.
- [11] Ting Chen, Simon Kornblith, Mohammad Norouzi, and Geoffrey Hinton. A simple framework for contrastive learning of visual representations. In Hal Daumé III and Aarti Singh, editors, *Proceedings of the 37th International Conference on Machine Learning*, volume 119 of *Proceedings of Machine Learning Research*, pages 1597–1607. PMLR, 13–18 Jul 2020. URL <https://proceedings.mlr.press/v119/chen20j.html>.
- [12] Hoagy Cunningham, Aidan Ewart, Logan Riggs, Robert Huben, and Lee Sharkey. Sparse autoencoders find highly interpretable features in language models. *arXiv preprint arXiv:2309.08600*, 2023.
- [13] Pablo J Diego-Simón, Emmanuel Chemla, Jean-Rémi King, and Yair Lakretz. Probing syntax in large language models: Successes and remaining challenges. *arXiv preprint arXiv:2508.03211*, 2025.

- [14] Jacob Dunefsky, Philippe Chlenski, and Neel Nanda. Transcoders find interpretable llm feature circuits. *Advances in Neural Information Processing Systems*, 37:24375–24410, 2024.
- [15] Nelson Elhage, Neel Nanda, Catherine Olsson, and et al. A mathematical framework for transformer circuits. *Transformer Circuits Thread*, 2021. <https://transformer-circuits.pub/2021/framework/index.html>.
- [16] Cheng Gao, Yuan Cao, Zihao Li, Yihan He, Mengdi Wang, Han Liu, Jason Matthew Klusowski, and Jianqing Fan. Global convergence in training large-scale transformers. In *The Thirty-eighth Annual Conference on Neural Information Processing Systems*, 2024. URL <https://openreview.net/forum?id=9wt1fRKwZS>.
- [17] Tianyu Gao, Xingcheng Yao, and Danqi Chen. SimCSE: Simple contrastive learning of sentence embeddings. In Marie-Francine Moens, Xuanjing Huang, Lucia Specia, and Scott Wen-tau Yih, editors, *Proceedings of the 2021 Conference on Empirical Methods in Natural Language Processing*, pages 6894–6910, Online and Punta Cana, Dominican Republic, November 2021. Association for Computational Linguistics. doi: 10.18653/v1/2021.emnlp-main.552. URL <https://aclanthology.org/2021.emnlp-main.552/>.
- [18] Fabian Gloeckle, Badr Youbi Idrissi, Baptiste Rozière, David Lopez-Paz, and Gabriel Synnaeve. Better & faster large language models via multi-token prediction. *arXiv preprint arXiv:2404.19737*, 2024.
- [19] Aaron Gokaslan, Vanya Cohen, Ellie Pavlick, and Stefanie Tellex. Openwebtext corpus. <http://Skylion007.github.io/OpenWebTextCorpus>, 2019.
- [20] Aaron Grattafiori, Abhimanyu Dubey, Abhinav Jauhri, and et al. The llama 3 herd of models, 2024. URL <https://arxiv.org/abs/2407.21783>.
- [21] Wes Gurnee and Max Tegmark. Language models represent space and time. In *The Twelfth International Conference on Learning Representations*, 2024. URL <https://openreview.net/forum?id=jE8xbmvFin>.
- [22] David Ha and Jürgen Schmidhuber. Recurrent world models facilitate policy evolution. *Advances in neural information processing systems*, 31, 2018.
- [23] Danijar Hafner, Timothy Lillicrap, Jimmy Ba, and Mohammad Norouzi. Dream to control: Learning behaviors by latent imagination. *arXiv preprint arXiv:1912.01603*, 2019.
- [24] Dean S Hazineh, Zechen Zhang, and Jeffery Chiu. Linear latent world models in simple transformers: A case study on othello-gpt. *arXiv preprint arXiv:2310.07582*, 2023.
- [25] John Hewitt and Percy Liang. Designing and interpreting probes with control tasks. In Kentaro Inui, Jing Jiang, Vincent Ng, and Xiaojun Wan, editors, *Proceedings of the 2019 Conference on Empirical Methods in Natural Language Processing and the 9th International Joint Conference on Natural Language Processing (EMNLP-IJCNLP)*, pages 2733–2743, Hong Kong, China, November 2019. Association for Computational Linguistics. doi: 10.18653/v1/D19-1275. URL <https://aclanthology.org/D19-1275/>.
- [26] Abhinav Kumar, Chenhao Tan, and Amit Sharma. Probing classifiers are unreliable for concept removal and detection. *Advances in Neural Information Processing Systems*, 35:17994–18008, 2022.
- [27] Jenny Kunz and Marco Kuhlmann. Classifier probes may just learn from linear context features. In Donia Scott, Nuria Bel, and Chengqing Zong, editors, *Proceedings of the 28th International Conference on Computational Linguistics*, pages 5136–5146, Barcelona, Spain (Online), December 2020. International Committee on Computational Linguistics. doi: 10.18653/v1/2020.coling-main.450. URL <https://aclanthology.org/2020.coling-main.450/>.
- [28] Yann LeCun. A path towards autonomous machine intelligence version 0.9. 2, 2022-06-27. *Open Review*, 62(1): 1–62, 2022.
- [29] Kenneth Li, Aspen K Hopkins, David Bau, Fernanda Viégas, Hanspeter Pfister, and Martin Wattenberg. Emergent world representations: Exploring a sequence model trained on a synthetic task. In *The Eleventh International Conference on Learning Representations*, 2023. URL [https://openreview.net/forum?id=DeG07\\_TcZvT](https://openreview.net/forum?id=DeG07_TcZvT).

- [30] Percy Liang, Rishi Bommasani, Tony Lee, Dimitris Tsipras, Dilara Soylu, Michihiro Yasunaga, Yian Zhang, Deepak Narayanan, Yuhuai Wu, Ananya Kumar, et al. Holistic evaluation of language models. *arXiv preprint arXiv:2211.09110*, 2022.
- [31] Tianyang Lin, Yuxin Wang, Xiangyang Liu, and Xipeng Qiu. A survey of transformers. *AI Open*, 3:111–132, 2022. ISSN 2666-6510. doi: <https://doi.org/10.1016/j.aiopen.2022.10.001>. URL <https://www.sciencedirect.com/science/article/pii/S2666651022000146>.
- [32] Zhenru Lin, Jiawen Tao, Yang Yuan, and Andrew Chi-Chih Yao. Existing llms are not self-consistent for simple tasks. *arXiv preprint arXiv:2506.18781*, 2025.
- [33] Jack Lindsey, Wes Gurnee, Emmanuel Ameisen, Brian Chen, Adam Pearce, Nicholas L. Turner, Craig Citro, David Abrahams, Shan Carter, Basil Hosmer, Jonathan Marcus, Michael Sklar, Adly Templeton, Trenton Bricken, Callum McDougall, Hoagy Cunningham, Thomas Henighan, Adam Jermyn, Andy Jones, Andrew Persic, Zhenyi Qi, T. Ben Thompson, Sam Zimmerman, Kelley Rivoire, Thomas Conerly, Chris Olah, and Joshua Batson. On the biology of a large language model. *Transformer Circuits Thread*, 2025. URL <https://transformer-circuits.pub/2025/attribution-graphs/biology.html>.
- [34] Bingbin Liu, Jordan T. Ash, Surbhi Goel, Akshay Krishnamurthy, and Cyril Zhang. Transformers learn shortcuts to automata. In *The Eleventh International Conference on Learning Representations*, 2023. URL <https://openreview.net/forum?id=De4FYqjFueZ>.
- [35] David Q Mayne, James B Rawlings, Christopher V Rao, and Pierre OM Scokaert. Constrained model predictive control: Stability and optimality. *Automatica*, 36(6):789–814, 2000.
- [36] Kevin Meng, David Bau, Alex J Andonian, and Yonatan Belinkov. Locating and editing factual associations in GPT. In Alice H. Oh, Alekh Agarwal, Danielle Belgrave, and Kyunghyun Cho, editors, *Advances in Neural Information Processing Systems*, 2022. URL <https://openreview.net/forum?id=-h6WAS6eE4>.
- [37] Ida Momennejad, Hosein Hasanbeig, Felipe Vieira Frujeri, Hiteshi Sharma, Nebojsa Jojic, Hamid Palangi, Robert Ness, and Jonathan Larson. Evaluating cognitive maps and planning in large language models with cogeval. In *Thirty-seventh Conference on Neural Information Processing Systems*, 2023. URL <https://openreview.net/forum?id=VtkGvGcGe3>.
- [38] Manfred Morari and Jay H. Lee. Model predictive control: past, present and future. *Computers & Chemical Engineering*, 23:667–682, 1999. URL <https://api.semanticscholar.org/CorpusID:19026701>.
- [39] Vaishnavh Nagarajan, Chen Henry Wu, Charles Ding, and Aditi Raghunathan. Roll the dice & look before you leap: Going beyond the creative limits of next-token prediction. In *Forty-second International Conference on Machine Learning*, 2025. URL <https://openreview.net/forum?id=Hi0SyHMmkd>.
- [40] Catherine et al. Olsson. In-context learning and induction heads. *Transformer Circuits Thread*, 2022. <https://transformer-circuits.pub/2022/in-context-learning-and-induction-heads/index.html>.
- [41] Koyena Pal, Jiuding Sun, Andrew Yuan, Byron Wallace, and David Bau. Future lens: Anticipating subsequent tokens from a single hidden state. In Jing Jiang, David Reitter, and Shumin Deng, editors, *Proceedings of the 27th Conference on Computational Natural Language Learning (CoNLL)*, pages 548–560, Singapore, December 2023. Association for Computational Linguistics. doi: 10.18653/v1/2023.conll-1.37. URL <https://aclanthology.org/2023.conll-1.37/>.
- [42] Tiago Pimentel, Josef Valvoda, Rowan Hall Maudslay, Ran Zmigrod, Adina Williams, and Ryan Cotterell. Information-theoretic probing for linguistic structure. In Dan Jurafsky, Joyce Chai, Natalie Schluter, and Joel Tetreault, editors, *Proceedings of the 58th Annual Meeting of the Association for Computational Linguistics*, pages 4609–4622, Online, July 2020. Association for Computational Linguistics. doi: 10.18653/v1/2020.acl-main.420. URL <https://aclanthology.org/2020.acl-main.420/>.

- [43] Abhilasha Ravichander, Yonatan Belinkov, and Eduard Hovy. Probing the probing paradigm: Does probing accuracy entail task relevance? In *Proceedings of the 16th Conference of the European Chapter of the Association for Computational Linguistics: Main Volume*, pages 3363–3377, 2021.
- [44] Jonathan Richens, Tom Everitt, and David Abel. General agents need world models. In *Forty-second International Conference on Machine Learning*, 2025. URL <https://openreview.net/forum?id=d1IoumNiXt>.
- [45] Yash Saxena, Sarthak Chopra, and Arunendra Mani Tripathi. Evaluating consistency and reasoning capabilities of large language models. In *2024 Second International Conference on Data Science and Information System (ICDSIS)*, pages 1–5. IEEE, 2024.
- [46] Bilgehan Sel, Ruoxi Jia, and Ming Jin. LLMs can plan only if we tell them. In *The Thirteenth International Conference on Learning Representations*, 2025. URL <https://openreview.net/forum?id=K3Kr0sR6y9>.
- [47] Adam Shai, Paul M. Riechers, Lucas Teixeira, Alexander Gietelink Oldenziel, and Sarah Marzen. Transformers represent belief state geometry in their residual stream. In *The Thirty-eighth Annual Conference on Neural Information Processing Systems*, 2024. URL <https://openreview.net/forum?id=YIB7REL8UC>.
- [48] Yongliang Shen, Kaitao Song, Xu Tan, Dongsheng Li, Weiming Lu, and Yueting Zhuang. Hugginggpt: Solving ai tasks with chatgpt and its friends in hugging face. *Advances in Neural Information Processing Systems*, 36: 38154–38180, 2023.
- [49] Ravid Shwartz-Ziv and Naftali Tishby. Opening the black box of deep neural networks via information. *arXiv preprint arXiv:1703.00810*, 2017.
- [50] Oscar Skean, Md Rifat Arefin, Dan Zhao, Niket Nikul Patel, Jalal Naghiyev, Yann LeCun, and Ravid Shwartz-Ziv. Layer by layer: Uncovering hidden representations in language models. In *Forty-second International Conference on Machine Learning*, 2025. URL <https://openreview.net/forum?id=WGXb7UdvTX>.
- [51] Aarohi Srivastava, Abhinav Rastogi, Abhishek Rao, and et al. Beyond the imitation game: Quantifying and extrapolating the capabilities of language models. *Transactions on Machine Learning Research*, 2023. ISSN 2835-8856. URL <https://openreview.net/forum?id=uyTL5Bvosj>. Featured Certification.
- [52] Jianlin Su, Murtadha Ahmed, Yu Lu, Shengfeng Pan, Wen Bo, and Yunfeng Liu. Roformer: Enhanced transformer with rotary position embedding. *Neurocomputing*, 568:127063, 2024.
- [53] Sainbayar Sukhbaatar, Édouard Grave, Piotr Bojanowski, and Armand Joulin. Adaptive attention span in transformers. In *Proceedings of the 57th Annual Meeting of the Association for Computational Linguistics*, pages 331–335, 2019.
- [54] Naftali Tishby and Noga Zaslavsky. Deep learning and the information bottleneck principle. In *2015 IEEE information theory workshop (itw)*, pages 1–5. Ieee, 2015.
- [55] Hugo Touvron, Louis Martin, Kevin Stone, Peter Albert, Amjad Almahairi, Yasmine Babaei, Nikolay Bashlykov, Soumya Batra, Prajjwal Bhargava, Shruti Bhosale, et al. Llama 2: Open foundation and fine-tuned chat models. *arXiv preprint arXiv:2307.09288*, 2023.
- [56] Muhammed Ustaomeroglu and Guannan Qu. A theoretical study of (hyper) self-attention through the lens of interactions: Representation, training, generalization. In *Forty-second International Conference on Machine Learning*, 2025. URL <https://openreview.net/forum?id=wQvR1LHboD>.
- [57] Aaron Van Den Oord, Oriol Vinyals, et al. Neural discrete representation learning. *Advances in neural information processing systems*, 30, 2017.
- [58] E Voita and I Titov. Information-theoretic probing with minimum description length. In *EMNLP 2020-2020 Conference on Empirical Methods in Natural Language Processing, Proceedings of the Conference*, pages 183–196, 2020.

- [59] Elena Voita, Rico Sennrich, and Ivan Titov. The bottom-up evolution of representations in the transformer: A study with machine translation and language modeling objectives. In Kentaro Inui, Jing Jiang, Vincent Ng, and Xiaojun Wan, editors, *Proceedings of the 2019 Conference on Empirical Methods in Natural Language Processing and the 9th International Joint Conference on Natural Language Processing (EMNLP-IJCNLP)*, pages 4396–4406, Hong Kong, China, November 2019. Association for Computational Linguistics. doi: 10.18653/v1/D19-1448. URL <https://aclanthology.org/D19-1448/>.
- [60] Guanzhi Wang, Yuqi Xie, Yunfan Jiang, Ajay Mandlekar, Chaowei Xiao, Yuke Zhu, Linxi Fan, and Anima Anandkumar. Voyager: An open-ended embodied agent with large language models. *Transactions on Machine Learning Research*, 2024. ISSN 2835-8856. URL <https://openreview.net/forum?id=ehfRiF0R3a>.
- [61] Kevin Ro Wang, Alexandre Variengien, Arthur Conmy, Buck Shlegeris, and Jacob Steinhardt. Interpretability in the wild: a circuit for indirect object identification in GPT-2 small. In *The Eleventh International Conference on Learning Representations*, 2023. URL <https://openreview.net/forum?id=NpsVSN6o4u1>.
- [62] Siwei Wang, Yifei Shen, Shi Feng, Haoran Sun, Shang-Hua Teng, and Wei Chen. ALPINE: Unveiling the planning capability of autoregressive learning in language models. In *The Thirty-eighth Annual Conference on Neural Information Processing Systems*, 2024. URL <https://openreview.net/forum?id=WfbZusv14E>.
- [63] Xinyi Wang, Lucas Caccia, Oleksiy Ostapenko, Xingdi Yuan, William Yang Wang, and Alessandro Sordani. Guiding language model reasoning with planning tokens. In *First Conference on Language Modeling*, 2024. URL <https://openreview.net/forum?id=wi9IffRhVM>.
- [64] Jason Wei, Xuezhi Wang, Dale Schuurmans, Maarten Bosma, Fei Xia, Ed Chi, Quoc V Le, Denny Zhou, et al. Chain-of-thought prompting elicits reasoning in large language models. *Advances in neural information processing systems*, 35:24824–24837, 2022.
- [65] Shunyu Yao, Dian Yu, Jeffrey Zhao, Izhak Shafran, Tom Griffiths, Yuan Cao, and Karthik Narasimhan. Tree of thoughts: Deliberate problem solving with large language models. *Advances in neural information processing systems*, 36:11809–11822, 2023.
- [66] Wenhao Zhao, Qiran Zou, Rushi Shah, and Dianbo Liu. Representation collapsing problems in vector quantization. In *Neurips Safe Generative AI Workshop 2024*, 2024. URL <https://openreview.net/forum?id=2a0EiTfcZ4>.
- [67] Zirui Zhao, Wee Sun Lee, and David Hsu. Large language models as commonsense knowledge for large-scale task planning. In *Thirty-seventh Conference on Neural Information Processing Systems*, 2023. URL <https://openreview.net/forum?id=Wjp1AYB81H>.
- [68] Yongxin Zhu, Bocheng Li, Yifei Xin, Zhihua Xia, and Linli Xu. Addressing representation collapse in vector quantized models with one linear layer, 2025. URL <https://arxiv.org/abs/2411.02038>.

## A Method details

In this section, we explain the details of our method and implementation.

### A.1 VQ-VAE design and implementation

Let  $h_t^\ell \in \mathbb{R}^d$  denote the hidden activation at token position  $t$  after Transformer layer  $\ell$ . We view a computation block as a set of layer-token indices  $S \subseteq \{1, \dots, L\} \times \{1, \dots, T\}$  and write the corresponding activations as

$$G_S = \{h_t^\ell \mid (\ell, t) \in S\}.$$

The goal is to map the variable-shaped  $G_S$  to a discrete code  $z_S \in [K]$  with a vector-quantized variational autoencoder (VQ-VAE). These codes serve as coarse summaries that represent the computation block and make information-theoretic analysis feasible. We measure dependencies between computations using codes, for example  $I(Z_A; Z_B)$  for two blocks  $G_A$  and  $G_B$ , as in the main text § 2.

**Architecture overview.** We train separate VQ-VAEs for target  $S$  sets used in our analyses. Each VQ-VAE has an encoder  $E$  that takes  $G_S$  and outputs a latent vector  $r_S \in \mathbb{R}^{d_e}$ , a codebook  $\{e_k\}_{k=1}^K \subset \mathbb{R}^{d_e}$ , and a decoder  $D$  that reconstructs  $\tilde{G}_S$  from the selected codebook vector. Quantization uses nearest neighbors

$$k^* = \arg \min_{k \in [K]} \|r_S - e_k\|^2, \quad z_S \equiv k^*, \quad \tilde{r}_S \equiv e_{k^*},$$

and the straight-through estimator for backpropagation is used for the gradient flow in training.

**Design rules by input structure.** In our experiments, we select various  $S$  depending on the analysis, as described in § 3. Even within the same experiment,  $S$  can vary along the token axis because different samples may have different lengths. We design the encoder  $E$  and decoder  $D$  according to the structure of the hidden state blocks, which span the layer dimension, token index dimension, and hidden state vector dimension. Below we summarize the design specializations of  $E$  and  $D$  to explain how we handle challenges in the structure of the hidden state blocks.

- **Multiple layers at the same token index.** For each layer  $\ell \in \mathcal{L}$ , we first process the sequence  $\{h_t^\ell\}$  with a transformer encoder. The resulting representations are then stacked across the layer axis. An MLP maps the stacked representation from dimension  $|\mathcal{L}| \cdot d$  down to  $d_e$  in the encoder. In the decoder, starting from  $\tilde{r}_S$ , we follow exact reverse operations, e.g., dimensionality expansion instead of dimensionality reduction with MLP.
- **Multiple token indices at the same layer.** We treat  $\{h_t^\ell\}_{t \in \mathcal{T}}$  as a sequence and process it with a transformer encoder. To handle variable sequence lengths, the encoder either crops the sequence to a fixed window  $T_{\text{enc}}$  or appends  $m$  learned sentinel vectors and uses their outputs to form  $r_S$ . In the end, we concatenate representations across multiple time indices and apply an additional MLP for further processing to get the encoder output. In the decoder, we first upsample the time dimension by mapping  $\tilde{r}_S$  with an MLP to a maximum original sequence of length with  $d$ -dimensional vectors, then refine per-token reconstructions with a transformer encoder.
- **No token axis (single vector) or after reducing it as above.** When the input does not include the token dimension, or when it has been reduced as described above, we use only MLPs in both the encoder and decoder. The encoder outputs a single summary vector, and the decoder reconstructs the corresponding  $G_S$  shape.

## A.2 Training and losses of VQ-VAE

**Training setup.** We train each VQ-VAE on hidden state blocks  $G_S$  extracted from a fixed, pretrained LM  $\mathcal{M}$  over datasets used in our analyses. For each mini-batch, we sample sequences  $\mathbf{x}_{1:T}$ , feed  $\mathcal{M}$  with inputs to get hidden activations  $h_t^l$ , assemble the target blocks  $G_S$  according to the experiment. Then, we optimize encoder  $E$ , codebook  $\{e_k\}_{k=1}^K$ , and decoder  $D$  while keeping  $M$  frozen. This follows the standard VQ-VAE pipeline [57] adapted to variable-shape transformer hidden states.

**Objective.** Given an input block  $G_S$  and encoder output  $r_S = E(G_S) \in \mathbb{R}^{d_e}$ , we quantize by nearest neighbor

$$k^\star = \arg \min_{k \in [K]} \|r_S - e_k\|_2^2, \quad \tilde{r}_S = e_{k^\star},$$

and reconstruct  $\widehat{G}_S = D(\tilde{r}_S)$  with straight-through gradients for the quantizer [57]. The loss combines four parts

$$\mathcal{L} = \underbrace{\mathcal{L}_{\text{rec}}}_{\text{data fidelity}} + \underbrace{\lambda_q \mathcal{L}_{\text{vq}}}_{\text{quantization and commitment}} + \underbrace{\lambda_{\text{cos}} \mathcal{L}_{\text{cos}}}_{\text{codebook diversity}} + \underbrace{\lambda_{\text{ent}} \mathcal{L}_{\text{ent}}}_{\text{anti-collapse}}.$$

*Reconstruction* uses mean-squared error over the entries of  $G_S$ ,

$$\mathcal{L}_{\text{rec}} = \|G_S - \widehat{G}_S\|_2^2.$$

*Quantization and commitment* follow [57] with the straight-through estimator

$$\mathcal{L}_{\text{vq}} = \|\text{sg}[r_S] - e_{k^\star}\|_2^2 + \beta \|r_S - \text{sg}[e_{k^\star}]\|_2^2,$$

where  $\text{sg}[\cdot]$  is stop-gradient and  $\beta$  balances codebook learning and encoder commitment. *Codebook diversity* encourages distinct codes by discouraging cosine similarity among embeddings,

$$\mathcal{L}_{\text{cos}} = \frac{1}{K(K-1)} \sum_{i \neq j} \left( \frac{\langle e_i, e_j \rangle}{\|e_i\|_2 \|e_j\|_2} \right)^2,$$

which spreads codebook vectors and yields more discriminative high-level codes, consistent with our use of codes as discussed in main text § 2. To avoid mode collapse of VQ-VAE [66, 68], we further uses an *anti-collapse entropy* term which employs soft assignments computed from distances to the full codebook. Let

$$p_k = \frac{\exp(-\alpha \|r_S - e_k\|_2^2)}{\sum_{j=1}^K \exp(-\alpha \|r_S - e_j\|_2^2)},$$

then we minimize the negative entropy

$$\mathcal{L}_{\text{ent}} = -H(p) = -\sum_{k=1}^K p_k \log p_k,$$

which promotes higher-entropy assignments during training and discourages mode collapse.

**Stabilizing codebook usage.** VQ-VAE training can suffer from codebook collapse [66, 68]. We adopt three complementary heuristics. (i) *Dead-code reset*: codes that have not been the argmin  $k^\star$  for a fixed window are reinitialized to random encoder outputs from the current batch. (ii) *Codebook dropout*: with probability 0.1 we temporarily mask a random subset of codebook vectors when forming nearest-neighbor distances in the forward pass of training, which encourages redundancy avoidance and better exploration. (iii) *Entropy regularization*: the  $\mathcal{L}_{\text{ent}}$  term above explicitly pushes assignments away from degenerate peaks.

**Optimization details.** We use the Adam optimizer for training. Inputs at every token index and layer index are normalized before encoding.

**Evaluation metrics.** For quantitative checks of representation quality and nontrivial code usage, we report: (i)  $nRMSE$  between inputs and reconstructions. Let  $H$  denote a vectorized view of  $G_S$  and  $\widehat{H}$  that of  $\widehat{G}_S$ . With  $Z_H \in [K]$  the selected code and  $\widehat{H} = D(e_{Z_H})$ , define

$$nRMSE = \frac{\|H - \widehat{H}\|_2}{\|H\|_2}.$$

- (ii) *Codebook geometry*: cosine similarity among codebook vectors  $\{e_k\}_{k=1}^K$  and its distribution, which reflects diversity.
- (iii) *Usage distribution*: empirical frequencies of  $Z_H$ .

**Rationale for the objective.** The reconstruction term certifies that codes retain task-relevant information about  $G_S$ , the VQ term ties encoder outputs to discrete codes, the cosine penalty promotes discriminative summaries that support our information-theoretic analyses, and the entropy term plus stabilization heuristics sustain broad code usage throughout training.

### A.3 A Validation on a representative experiment

To validate our use of VQ-VAE-derived codes for estimating between computations, we define discrete variables  $(A, B)$ . Let  $A$  be uniform on a domain  $\mathcal{A}$  with  $|\mathcal{A}| = 1024$ , and let

$$\mathbb{P}(B = b \mid A = a) = \begin{cases} p_v & \text{if } b = a, \\ \frac{1-p_v}{1023} & \text{otherwise.} \end{cases}$$

The  $\mathcal{I}(A; B)$  admits a closed-form expression that depends on  $p_v$ . We treat  $(A, B)$  as the *ground-truth coarse variables* that our method aims to recover.

To mimic transformer computations, we associate each  $a \in \mathcal{A}$  with a hidden-state tensor  $G_A \in \mathbb{R}^{10 \times 11 \times 768}$  capturing all block outputs except the final layer of a trained GPT-3 small sized model given a random prefix of length 10. Also, we associate each possible value of  $B$  with  $G_B \in \mathbb{R}^{768}$ , the final-layer hidden state at a single position. These tensors are *redundant surrogates* for  $(A, B)$  in the sense that they only contain 10-bit information, i.e.,  $\log_2 1024$ , despite their huge dimensions, which match the largest hidden-state structures used in our experimental analysis.

We then apply our pipeline: train VQ-VAE models on  $G_A$  and  $G_B$  to obtain discrete codes  $Z_A$  and  $Z_B$ , which serve as coarse summaries of the corresponding computations. Finally, we compare  $\mathcal{I}(Z_A; Z_B)$  to the ground-truth  $\mathcal{I}(A; B)$  across values of  $p_v$  and across codebook sizes  $K$ . Figure 4 reports both  $\mathcal{I}(A; B)$  and  $\mathcal{I}(Z_A; Z_B)$  normalized within each  $K$ . For every  $K$ , the codes preserve the ordering induced by the ground-truth, and  $\mathcal{I}(Z_A; Z_B)$  approaches the ground truth as  $K$  increases. We do not train to recover  $(A, B)$ , so  $\mathcal{I}(A; B)$  is not a supervised target. Rather,  $\mathcal{I}(A; B)$  is a *reference-process MI* that comes from the constructed latent variables defining the generative story behind  $(G_A, G_B)$ .

## B Details of experimental analyses

We provide details of experimental settings and analyses here.

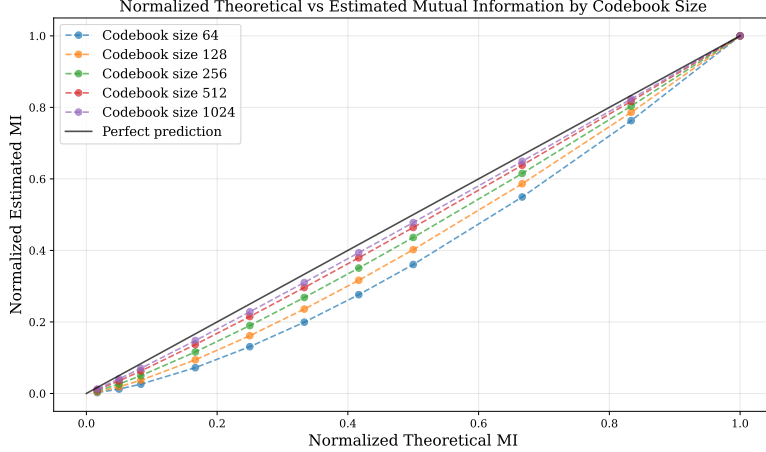


Figure 4: The comparison of our normalized latent mutual information estimations with different codebook sizes.

## B.1 Loss functions

Let  $\mathcal{V}$  be the vocabulary. A sequence is  $\mathbf{x} = (x_1, \dots, x_T)$  with prefixes  $x_{\leq t}$ . The model  $\mathcal{M}$  has embedding  $E \in \mathbb{R}^{|\mathcal{V}| \times d}$  and a shared unembedding  $U \in \mathbb{R}^{|\mathcal{V}| \times d}$ . The transformer has  $L$  layers and width  $d$ . Hidden states are  $h_t^\ell \in \mathbb{R}^d$  for  $\ell = 1, \dots, L$  and  $t = 1, \dots, T$ ; we write  $h_t^L$  for the final-layer state. We use  $\mathbb{P}$  for probabilities and  $\log$  for natural logarithms.

**Next-token prediction (NTP).** With teacher forcing, the baseline objective maximizes the conditional likelihood of the immediate next token from the final-layer state  $h_t^L$ . We use a shared unembedding  $U \in \mathbb{R}^{|\mathcal{V}| \times d}$ :

$$\mathbb{P}_\theta(x_{t+1} | x_{\leq t}) = \text{softmax}(U h_t^L)_{x_{t+1}}, \quad \mathcal{L}_{\text{NTP}}(\theta) = - \sum_{t=1}^{T-1} \log \mathbb{P}_\theta(x_{t+1} | x_{\leq t}).$$

**Multi-token prediction (MTP).** To align internal states with short-horizon futures, we equip the model with  $\Gamma$  output heads [18]. Head  $\gamma \in \{1, \dots, \Gamma\}$  is implemented as a transformer layer  $f_h^{(\gamma)}: \mathbb{R}^d \rightarrow \mathbb{R}^d$  that takes  $h_t^L$  as input and is followed by the same shared unembedding  $U$ :

$$\mathbb{P}_\theta(x_{t+\gamma} | x_{\leq t}) = \text{softmax}\left(U f_h^{(\gamma)}(h_t^L)\right)_{x_{t+\gamma}}.$$

The training loss sums the cross-entropy across positions and horizons:

$$\mathcal{L}_{\text{MTP}}(\theta) = - \sum_{t=1}^{T-\Gamma} \sum_{\gamma=1}^{\Gamma} \log \mathbb{P}_\theta(x_{t+\gamma} | x_{\leq t}).$$

All heads contribute equally. At test time decoding remains autoregressive; the auxiliary heads affect only the training signal and can optionally be used for speedups.

In our experiments, when we use MTP loss in CFG task, we used  $\Gamma = 4$ . As for, PF-Long and PF-Short tasks we used  $\Gamma = 2$

## B.2 Dataset

Here we explain how we generated the dataset and how we used them in our LM training.

### B.2.1 Context-free grammar data generation details

The specific formal details of our CFG are not central to the claims of this paper. We use it only as a controlled source of long, purely syntactic sequences. Readers who want a formal presentation and broader context can consult the CFG-based data generation reference [4], on which our CFG data is based on. Here we provide the details of our specific CFG parallel to the naming convention in [4].

We construct a layered grammar that expands strictly downward from a single start symbol to a set of terminals. The layers are organized as one start symbol, then four intermediate nonterminal layers of size three each, and finally a terminal inventory of sixty four symbols, summarized as the tuple (1, 4, 4, 4, 64). For every nonterminal we define a small menu of alternative productions; each nonterminal has between three and five alternatives, and each alternative rewrites the parent into two or three symbols drawn only from the next layer. This acyclic layout fixes the depth of any derivation and guarantees termination.

Once the grammar is fixed, each sequence is produced by starting at the start symbol and repeatedly expanding pending nonterminals until only terminals remain. Whenever a nonterminal has several alternatives, one is chosen at random. Because expansion always moves one layer down, sequences are long but tightly controlled in length. In the configuration used in the paper we generate four million sequences. The shortest contains 16 terminals and the longest 67 (the number of terminals corresponds to the sequence length), measured without begin or end markers. The resulting corpus contains 4M sequences (150M tokens).

### B.2.2 Path-finding data generation details

PF-Short is built to be a small but nontrivial path-finding task. In every instance the start node is labeled 1 and the goal node is labeled 2. We first lay down two *correct* trunks from the start to the goal. Each trunk has exactly two internal nodes, so a correct answer has the form 1, a, b, 2. We then lay down two *decoy* trunks that also begin at the start but end at fresh terminals that are not the goal. Decoys are the same length as the correct trunks, and the interiors of all trunks are disjoint. Up to this point the graph contains the start, the goal, two correct routes that meet only at those endpoints, and two look-alike alternatives that never reach the goal.

To make the local neighborhood around each trunk less revealing, we sprinkle branches on top of the trunks. We do this in one layer: for each eligible trunk node we independently add a small number of fresh children drawn from a Poisson distribution with mean one, and we cap the number of branch children per node at two. We never branch from the goal or from decoy terminals, and for the start node we reduce its branch allowance to account for the four trunk edges already attached to it, so its total degree remains bounded. If the instance would exceed the node budget of 28 distinct labels we discard it and resample.

Before writing the example to disk we randomly relabel every internal node using a permutation of the labels 3 through 28, while keeping 1 and 2 fixed. We also shuffle the edge list. The model never sees coordinates or orders, only an unordered set of undirected edges and an answer slot. A simplified typical prompt looks like

1 9, 7 2, 9 5, 1 3, 3 7, 5 2:

and either 1 9 5 2 or 1 3 7 2 is accepted as correct. In our experiments the PF-Short training split contains 16M samples

generated with the recipe above. We also have a similar sized dataset to train corresponding vqvae and a smaller validation data. Please also refer to Figure 1 (right) for a simplified network example.

PF-Long extends the horizon while keeping local clutter modest. We again fix the start to 1 and the goal to 2. We lay down two correct trunks, each with four internal nodes, so a correct answer has the form 1, a, b, c, d, 2. We then add one decoy trunk of the same length that begins at 1 but ends at a fresh non-goal terminal; interiors are disjoint. To add distractors we apply a two-layer branching pass: a light first layer around trunks followed by a very light second layer, with at most one branch child per parent. We never branch from the goal or from decoy terminals, and we reduce the start’s branch allowance to respect the degree cap. If a sample would exceed the budget of 28 distinct node labels we discard and resample. Finally we randomly permute the internal labels within 3 through 28, keep 1 and 2 fixed, remap the paths, and shuffle the edge list. The training split contains 16M PF-Long examples generated with this recipe.

### B.2.3 Natural language (OpenWebText)

Finally, we include a large-scale natural language dataset (OpenWebText) to examine whether our information-theoretic analyses extend to unconstrained real-world data. Unlike the synthetic CFG or path-finding settings, this dataset reflects distributional structure from natural language and allows us to test whether planning signals identified in controlled tasks also emerge under standard pretraining conditions.

### B.2.4 How the generated data are used to train the language models

For the CFG and OpenWebText corpora we run conventional pretraining in separate setups. For CFG, we first generate many standalone sequences that satisfy the grammar. We then randomly shuffle these CFG sequences and concatenate them end to end to form a single text stream for that corpus. Training samples are taken by choosing a random starting offset in the CFG stream and slicing a fixed-length block equal to the model context window; the loss is computed on all tokens in the block except any optional boundary markers.

For OpenWebText, we apply the same pretraining recipe but within its own corpus only: documents are shuffled and concatenated to form an OpenWebText stream, blocks are sampled at random offsets, and next-token prediction is used with causal masking. There is no mixing or interleaving between CFG and OpenWebText at any stage.

For the path-finding data we use supervised finetuning rather than corpus streaming. Each example is a self-contained prompt and answer: the input is the unordered edge list written as comma-separated node pairs followed by a colon, and the target is any valid shortest path from the fixed start to the fixed goal. We concatenate prompt and answer for teacher forcing, mask the prompt so the loss is applied only to the answer span, and we do not concatenate different path-finding examples or split one across blocks. Under this scheme we use both PF-Short and PF-Long, whose correct answers have lengths four and six respectively when counting the start and goal.

## B.3 Details of planning horizon experiment (3.1)

**Details about VQ-VAE.** The VQ-VAE used to quantize the prefix representation  $H \in \mathbb{R}^{T \times L \times d}$  employs a 256-entry codebook ( $Z_H \in \{0, 1, \dots, 255\}$ ), while each future final-layer state  $h_\tau^L \in \mathbb{R}^d$  is quantized with a 64-entry codebook ( $Z_{h_{T+\tau}^L} \in \{0, 1, \dots, 63\}$ ).

For the CFG task, the dimension of  $H$  is on average  $16 \times 11 \times 768 = 135,168$ , and the dimension of  $h_\tau^L$  is 768. The mean nRMSE values of VQ-VAE encoding  $H$  into summary codes is 0.47, and that of encoding  $h_\tau^L$  is 0.21. Representative

codebook similarity and usage plots from VQ-VAE training to encode  $H$  for the CFG task are provided in Figure 5 and Figure 6. Also, those of VQ-VAE to encode  $h_\tau^L$  for the CFG task are provided in Figure 7 and Figure 8

For the PF-Short task, the dimension of  $H$  is on average  $70 \times 11 \times 768 = 591,360$ , and the dimension of  $h_\tau^L$  is 768. The mean nRMSE values of VQ-VAE encoding  $H$  into summary codes is 0.75, and that of encoding  $h_\tau^L$  is 0.48.

For the PF-Long task, to reduce dimensionality, we subsample every three layers when encoding  $H$  due to the limited model size, and we discard token indices corresponding to comma (,) tokens. The dimension of  $H$  is on average  $54 \times 4 \times 768 = 165,888$ , and the dimension of  $h_\tau^L$  is 768. The mean nRMSE values of VQ-VAE encoding  $H$  into summary codes is 0.59, and that of encoding  $h_\tau^L$  is 0.49.

*We emphasize that these are the results of huge quantization mappings, e.g., from 591,360 real numbers to 256 discrete labels.*

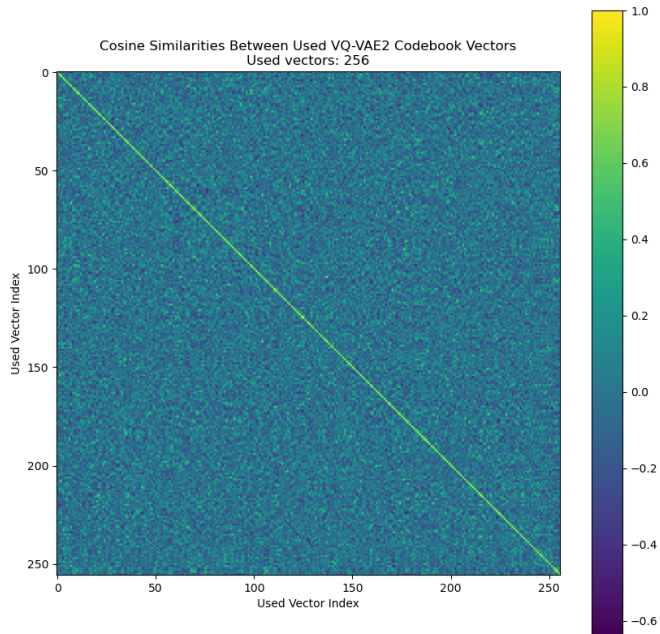


Figure 5: The codebook similarities for VQ-VAE encoding  $H$  in CFG task.

## B.4 Details of branches in the plan experiment (3.2)

**Details about VQ-VAE.** For the VQ-VAE details encoding  $H$  in PF-Short and PF-Long tasks, please, refer to the relevant part of App. B.3 since the same models are used.

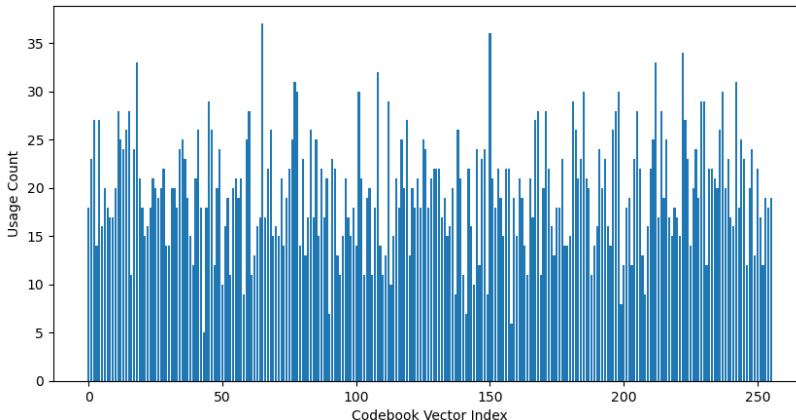


Figure 6: The codebook usage for VQ-VAE encoding  $H$  in CFG task.

**Encoding the paths.** The paths themselves does not have a vector representation and it is challenging use a unique class each possible path since in PF-Long, there can be  $28^4$  paths. Although PF-Short is relatively easier, we reduce the number of possible codes to 512 by training VQ-VAE over a learned embedding vector for each of 28 tokens. Then we obtain the high-level codes of full path using the trained VQ-VAE. For PF-Long, we calculate the MI between the  $H$ 's code obtained from VQ-VAE and each intermediate token (using the token's index itself) along the response path. Then, we take the mean of these values over the nodes on the path to get a full-path MI result.

## B.5 Details of the history in the plan experiment

### B.5.1 nMI results in § B.5 for longer-horizon generated tokens (higher $\tau$ )

We provide the results in Figures 9&10.

### B.5.2 Details of the conditional nMI estimates

To estimate  $I(Z_{T-15:T-1}^\ell; Z_T^\ell | Z_T^\ell)$ , we used the identity:

$$I(Z_{T-15:T-1}^\ell; Z_T^\ell | Z_T^\ell) = I(Z_{T-15:T}^\ell; Z_T^\ell) - I(Z_{T-15:T-1}^\ell; Z_T^\ell), \quad (3)$$

which holds because

$$Z_{T-15:T}^\ell = \{Z_{T-15:T-1}^\ell, Z_T^\ell\}.$$

The first term of the right hand side of (3), is already estimated and shown in the Figure 3 ( $k = 1$  block estimates). As for the second term, we find an approximate value as follows. First, because of the underlying task's symmetry (it is OpenWebtext, pretraining task), we have translational invariance, so

$$I(Z_{T-15:T-1}^\ell; Z_T^\ell) = I(Z_{T-14:T}^\ell; Z_{T+1}^\ell). \quad (4)$$

Then, we approximate the right-hand side of this equation by

$$I(Z_{T-14:T}^\ell; Z_{T+1}^\ell) \approx I(Z_{T-15:T}^\ell; Z_{T+1}^\ell),$$

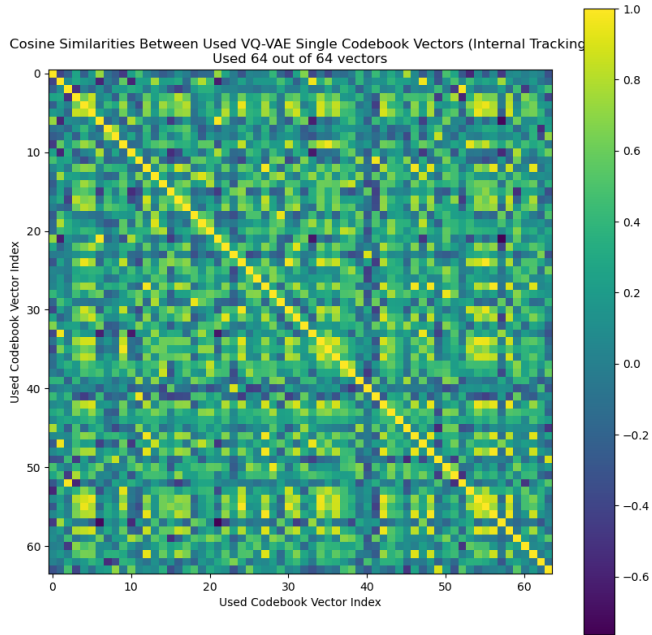


Figure 7: The codebook similarities for VQ-VAE encoding  $H$  in CFG task.

which relies on the observation that in natural language, the incremental information contributed by extending the context diminishes: as sentences become longer, the mutual information between past tokens and future ones grows only logarithmically.

### B.5.3 Details about Block VQ-VAE.

The VQ-VAE used to quantize  $\ell^{th}$  layer  $k^{th}$  block representation  $h_{T-16B:T+16-16B}^\ell \in \mathbb{R}^{16 \times d}$  employs a 1024-entry codebook ( $\mathbf{B}_k^\ell \in \{0, 1, \dots, 1023\}$ ), while each future final-layer state  $h_\tau^L \in \mathbb{R}^d$  is quantized with a 64-entry codebook ( $Z_{h_{T+\tau}^L} \in \{0, 1, \dots, 63\}$ ). Recall this experiment is on NLP (OpenWebText pretraining). The dimension of  $h_{T-16B:T+16-16B}^\ell$  is on average  $16 \times 512 = 7680$ , and the dimension of  $h_\tau^L$  is 512. The overall VQ-VAE for the blocks has 4M parameters in total. Representative codebook similarity and usage plots from VQ-VAE training to encode  $h_{T-16B:T+16-16B}^\ell$  for the (OpenWebText) task are provided in Figure 11 and Figure 12. For additional details on VQ-VAE trainings on OpenWebText (NLP pretraining) data please refer to App. B.6.

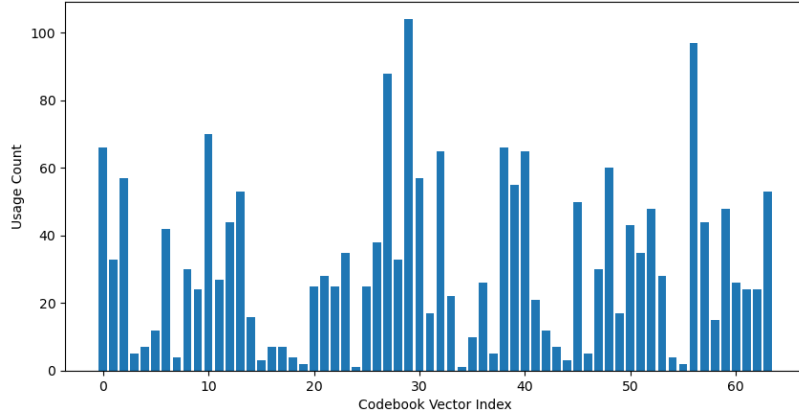


Figure 8: The codebook usage for VQ-VAE encoding  $H$  in CFG task.

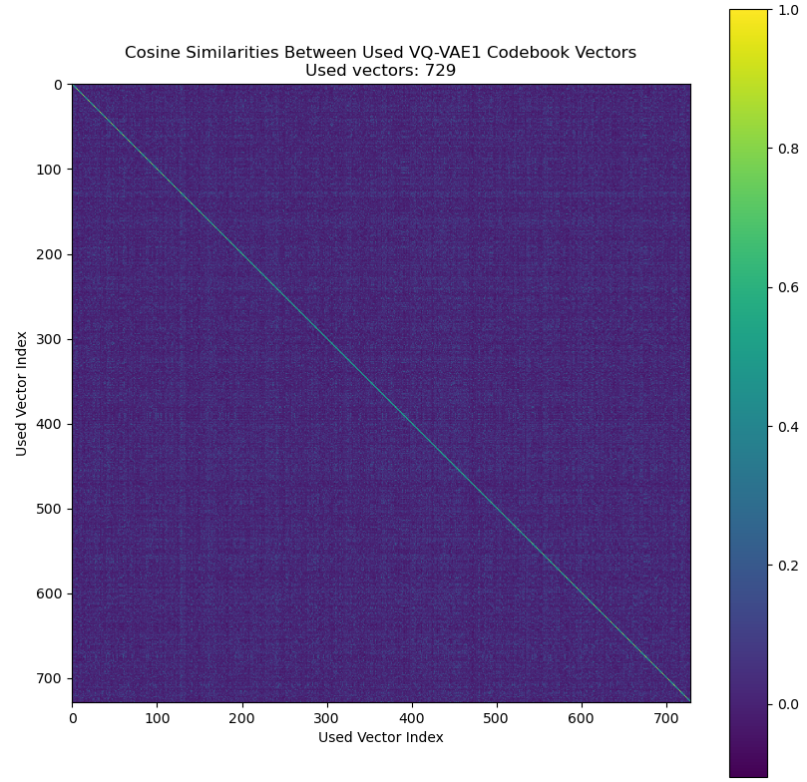


Figure 11: The codebook similarities for VQ-VAE encoding  $h_{T-16B:T+16-16B}^\ell$  in OpenWebText task.

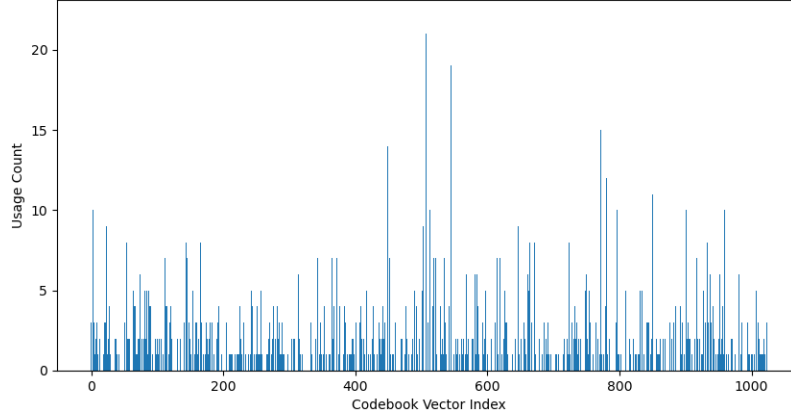


Figure 12: The codebook usage for VQ-VAE encoding  $h_{T-16B:T+16-16B}^{\ell}$  in OpenWebText task.

## B.6 On the scalability of our pipeline

Recall that to obtain the code  $Z_{T+\tau}^L$ , we use an encoder whose input is  $h_{T+\tau}^L$ . To study this, we trained VQ-VAEs of increasing sizes on OpenWebText, with a fixed codebook size of 64 vectors. OpenWebText is widely used for NLP pretraining, but the data lacks a strong coherent structure across samples. As a result, it is natural, and in fact expected, that reconstruction errors remain relatively high.

Figure 13 reports the normalized nRMSE as a function of model size. This hints that scaling the encoder can improve representation quality despite the inherent noisiness of the dataset.

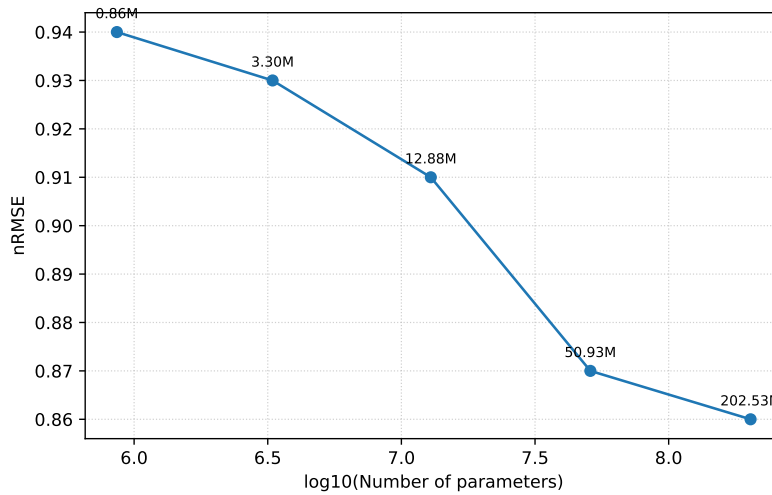


Figure 13: The nRMSE vs VQ-VAE encoder parameter count plot.

## C Related work in detail

We provide a longer discussion of the Related Work in the main text § 1.

**Language model planning.** In order to improve LMs’ reasoning and planning abilities, researchers have developed scaffolding and augmentation techniques, including Chain-of-Thought prompting [64], planning tokens [46, 63], and structured inference methods such as Tree-of-Thoughts and Graph-of-Thoughts [7, 65]. In parallel, hybrid systems that integrate LMs with symbolic planners or external tools have achieved state-of-the-art performance in embodied and tool-use domains [48, 60, 67]. Despite these advances, recent studies highlight that significant challenges remain, and current approaches to LM planning still fall short of fully addressing complex reasoning and decision-making tasks. For example, [32] show that models can produce conflicting answers under logically related prompts despite local plausibility, which shows lack of long horizon planning, although short-horizon planning works fine; [2] reveal discrepancies when asking a model what is correct vs what is incorrect; and [45] demonstrate that even repeated queries yield inconsistent outputs. Beyond inconsistency, some studies find that out-of-the-box models struggle with even simple planning tasks [37]. Complementing these empirical findings, theoretical analyses suggest that autoregressive models may face fundamental limits in their planning ability [62]. Taken together, these findings underscore that understanding whether and how planning arises in LMs is not only an open empirical challenge, but also central to both their interpretability and the principled design of future model architectures.

**Behavioral and Mechanistic Interpretability.** Some interpretability (explainability) methods consider the LM as black box, and design tasks or benchmarks to gauge reasoning, robustness, or generalization abilities [30, 51]. In contrast to them, mechanistic interpretability seeks to reverse-engineer transformer computations into human-understandable parts, treating the residual stream as the main information pathway and attention heads as separate components that pass information along [15]. Using this approach, researchers have explained key phenomena in LMs: in-context learning can arise from a characteristic two-head circuit that appears during a training “phase change,” with causal support from perturbation studies [40]; many neurons are polysemantic, but sparse autoencoders (SAEs) can replace them with more interpretable, monosemantic features that enable finer-grained causal analysis [8, 12]; models implicitly encode structural linguistic properties such as syntax [25]. Building on earlier approaches, transcoders, approximate dense MLPs with wider sparse layers, separating circuits into input-invariant and input-dependent components, and matching or surpassing SAEs in sparsity, faithfulness, and interpretability [14]. Frontier-scale case studies use cross-layer transcoders to trace multi-step reasoning and other behaviors, illustrating how these tools can audit mechanisms, not just features, in modern LLMs [33]. Overall, mechanistic interpretability offers concrete tools for uncovering how LLMs compute, though these methods are still developing.

**Mathematical Perspectives.** Beyond empirical tools, mathematically grounded perspectives also illuminate transformer/LLM interpretability: automata-theoretic analyses show self-attention can implement finite-state algorithms [34]; optimization views prove in-context learning corresponds to (preconditioned) gradient steps [3] and transformers are mutual interaction learners [56]; mean-field theory gives global convergence guarantees at scale [16].

**Probing.** A different line of interpretability work views LLM hidden states as structured representations that can be “probed”, probing refers to training lightweight models, often linear classifiers, to read out specific information from hidden states in order to test what the model represents internally. Using probing, researchers have shown that transformer hidden states encode structured belief-state and world-model-like information [21, 24, 47]. Other works demonstrate that a single hidden state can carry information about multiple future tokens [41] and that probing can reveal the underlying algorithms LLMs use to solve tasks [4].

However, standard accuracy-based probing has drawn a critique for combining what the probe can learn with and what the representation actually encodes making the results sensitive to probe capacity, data size, and hyperparameters [25, 42]. Further, high probe scores often come from exploiting superficial linear context cues rather than genuine structural knowledge [27]. Probing can even reveal features that a model does not use for its task [26, 43]. Consequently, some critiques motivate adopting information-theoretic lenses [13, 58]. Several approaches illustrate this perspective. The original Information Bottleneck framework [49, 54] casts learning as a trade-off between compressing input representations and preserving predictive information about outputs. Complementary work by Voita et al. [59] examined how information flows across transformer layers under different training objectives, revealing that tasks like language modeling, masked language modeling. More recently, Skean et al. [50] demonstrated that intermediate layers of LLMs often yield stronger representations than the final layer, using unified metrics based on entropy. and machine translation induce distinct patterns of information loss and reconstruction.

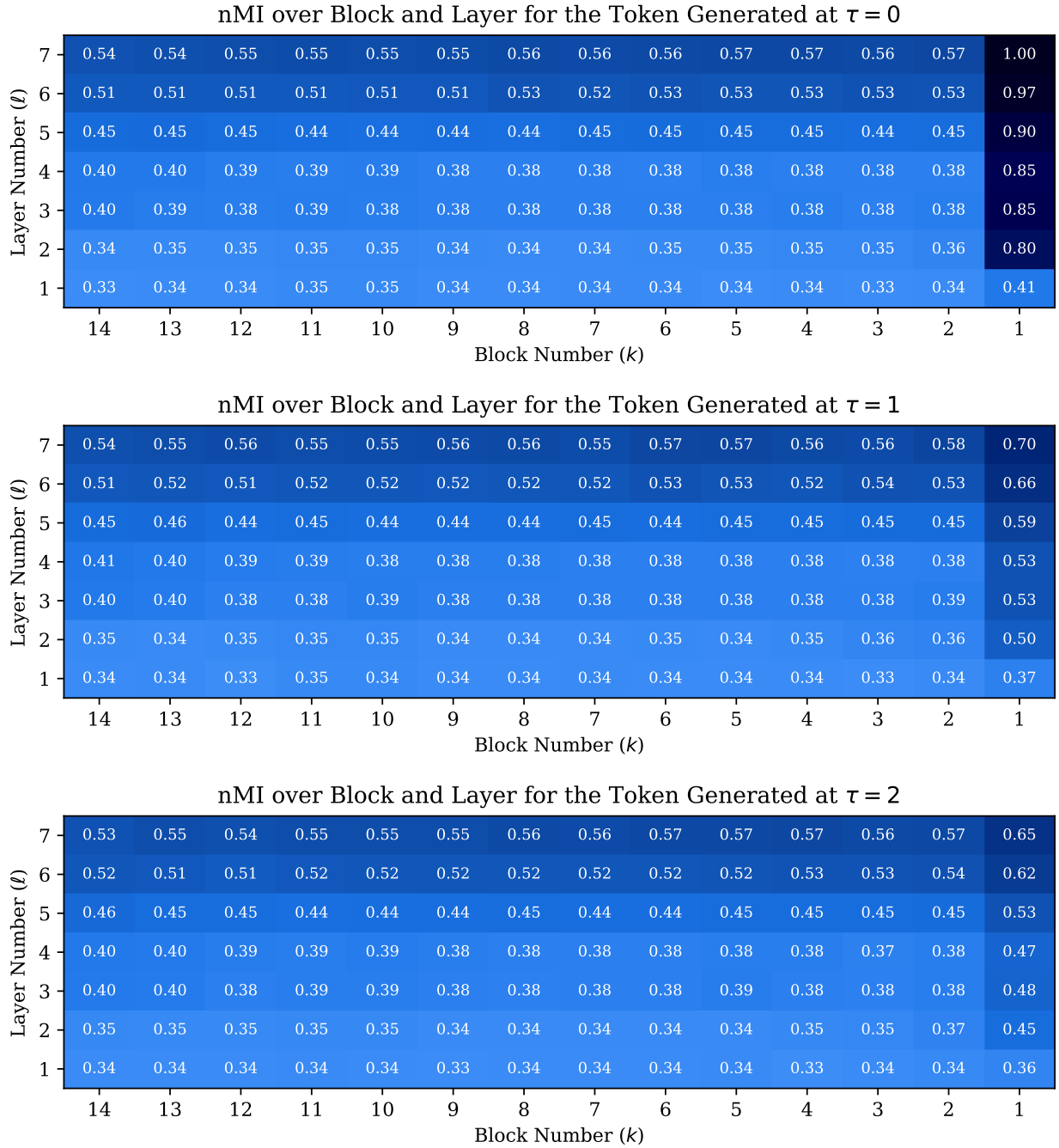


Figure 9: Heatmap of normalized mutual information over block and layer indices for  $\tau = 0, 1, 2$ . Please refer to the caption of 3.

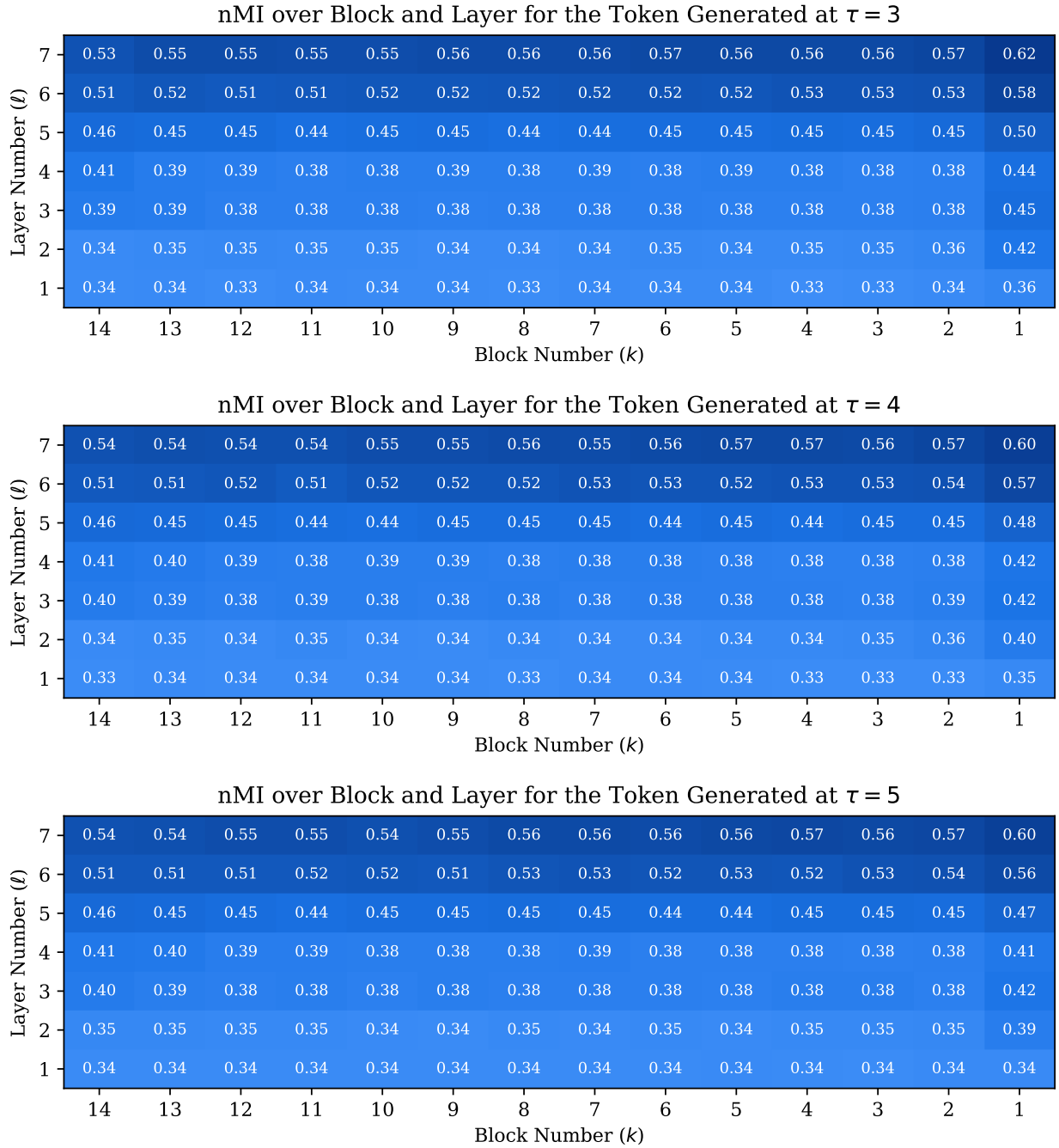


Figure 10: Heatmap of normalized mutual information over block and layer indices for  $\tau = 3, 4, 5$ . Please refer to the caption of 3.